IEEE control systems MAGAZINE

DECEMBER 2013 VOLUME 33 NUMBER 6

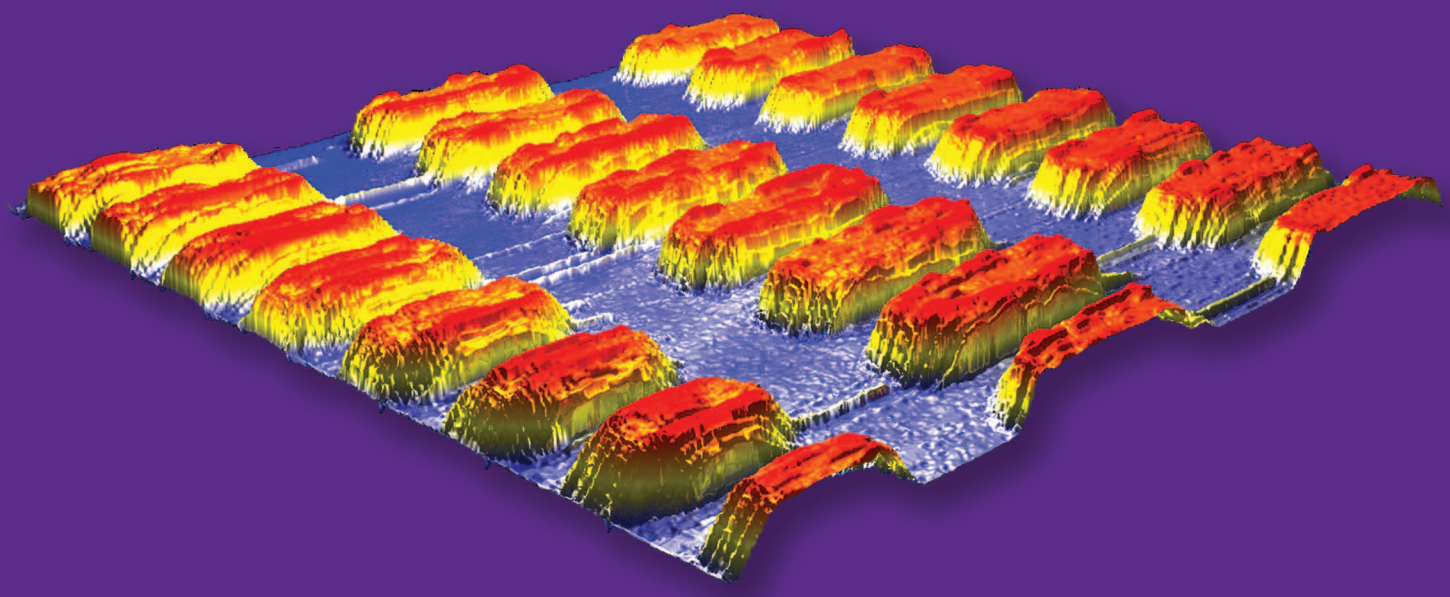

Micro- and Nanosystems

Control Systems Society
Advancing Control Science and Technology

IEEE

Micro- and Nanosystems

Micro- and nanoscale systems are a growing application area within the control systems field. Specific systems that have been investigated by control engineers include ink-jet printers [1], microseparation systems [2], [3], microchemical reactors [4]–[6], live cell positioning systems [7], drug delivery systems [2], [8], nanobio sensor arrays [2], data storage devices [9], optical switches [4], microlithography fabrication equipment [10], [11], atomic force microscopes (a.k.a. scanning probe microscopes) [12], [13], and microelectronic and nanoelectronic devices [2], [14]. While fundamental control principles are the same at any length scale, micro- and nanoscale pose some interesting challenges, such as greatly increasing stochasticity [2], [5], [7], greater physical limitations on actuator and sensor placement [4], and often more stringent limits on energy consumption [2], [5], [7].

Digital Object Identifier 10.1109/MCS.2013.2279417
Date of publication: 14 November 2013

This special issue is a collection of extended versions of papers presented at the Second Workshop on Dynamics and Control of Micro- and Nanoscale Systems held at the University of Newcastle, Australia, in February 2012. The opening article "Dynamics and Control of Micro- and Nanoscale Systems" by S.O. Reza Moheimani and Evangelos Eleftheriou provides an introduction to control problems in micro and nanoscale systems and summarizes the five feature articles in this issue.

In "Control Techniques for Increasing the Scan Speed and Minimizing Image Artifacts in Tapping-Mode Atomic Force Microscopy," Matthew W. Fairbairn and S.O. Reza Moheimani

Contributors

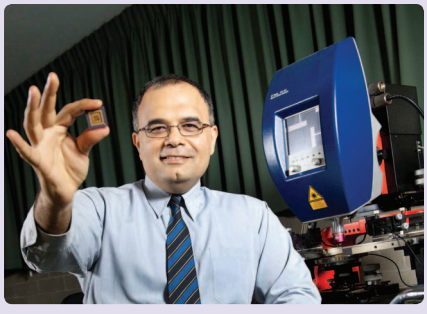

S.O. Reza Moheimani holding an on-chip atomic force microscope designed in his laboratory.

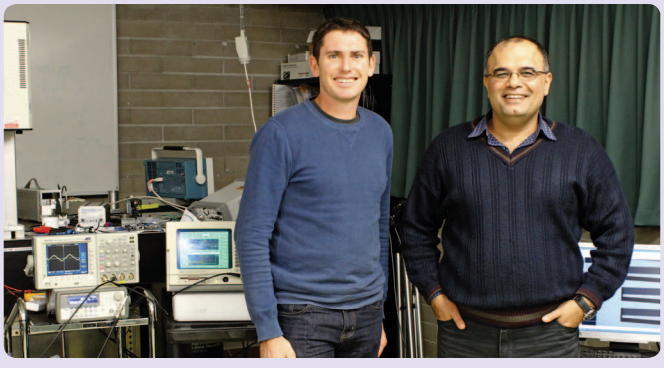

Matthew Fairbairn and S.O. Reza Moheimani in the control laboratory.

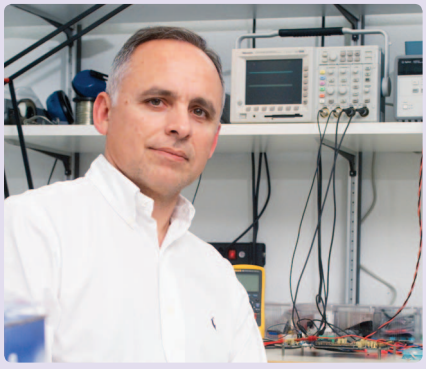

E. Eleftheriou in the laboratory.

John Lygeros (back) and (left to right) Tomas Tuma, Abu Sebastian, and Angeliki Pantazi, sitting next to their experimental nanopositioning system.

survey recent control design methods developed to improve the scan speed and the image resolution of intermittent-contact-mode atomic force microscopy, which is a technology used to generate multidimensional images of soft biological samples.

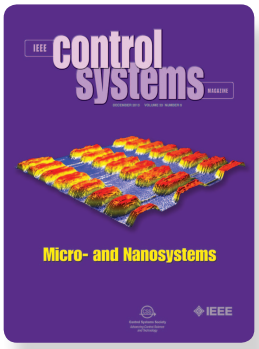

In "The Four Pillars of Nanopositioning for Scanning Probe Microscopy," Tomas Tuma, Abu Sebastian, John Lygeros, and Angeliki Pantazi provide an overview of recent progress in high-speed lateral nanopositioning using scanning probe microcopy. In "Design and Control for High-Speed Nanopositioning: Serial-Kinematic Nanopositioners and Repetitive Control for Nanofabrication," Yingfeng Shan and Kam K. Leang describe the control-oriented mechanical design of nanopositioning systems for high-speed tracking of periodic reference trajectories. In "AFM Imaging—Reliable or Not? Validation and Verification of Images in Atomic Force Microscopy," Srinivasa Salapaka, Aditya Ramamoorthy, and Murti V. Salapaka propose feedback-based strategies to correct for artifacts that can appear in images collected during contact-mode atomic force microscopy and consider the high-speed detection of topographical features.

In "Magnetic Navigation Control of Micro-agents in the Vascular Network: Challenges and Strategies for Endovascular Magnetic Navigation Control of Microscale Drug Delivery Carriers," Sylvain Martel describes a method for using a magnetic resonance imaging scanner to navigate microscale particles through the vascular network, such as a drug delivery carrier to a cancerous tumor. The motivation of this navigation is to maximize the effectiveness of expensive therapeutic compounds and to reduce harmful side effects.

In the "President's Message," Yutaka Yamamoto discusses internationalization and its benefits to the IEEE Control Systems Society (CSS) and provides closing remarks on the end of his term as CSS president. "CSS News" announces the upcoming availability of the Europe Control Conference proceedings on IEEE *Xplore*, a new program chair appointment, and information on the December 2013 CSS Board of Governors meeting. "CSS Business" provides the minutes of the CSS Board of Governors meeting held on June 16, 2013 in Washington, DC.

"Member Activities" provides information on the IEEE CSS Distinguished Lecturers program, which provides financial assitance for local groups to hold public lectures by

Yingfeng Shan in front of a waterfall.

Kam Leang on the summit of a mountain in the Lofoten Islands, Norway.

Aditya Ramamoorthy.

Srinivasa (Vasu) and Murti Salapaka hiking on Mount Diablo, near San Ramon, California.

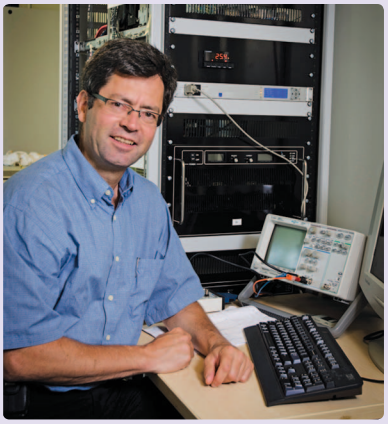

Sylvain Martel next to one of several electronic cabinets used for navigating micro-agents.

renowned control engineers. In "Technical Activities," Massoud Amin, Tariq Samad, and Jakob Stoustrup describe the recent activities of the CSS Technical Committee on Smart Grids. In "Publication Activities," Panos Antsaklis, the editor-in-chief of *IEEE Transactions on Automatic Control*, shares some thoughts about publishing results in the control field.

"People in Control" has interviews with incoming CSS President Jay Farrell and with IEEE Fellows Vincent Blondel, Eduardo Camacho, Tongwen Chen, Mustafa Khammash, Bozenna Pasik-Duncan, and Gang Tao. "Focus on Education" provides an example of a Matlab code that is sped up by more than three orders of magnitude by small but important changes in implementation.

This issue's "Historical Perspectives" column is the third in a series that commemorates the life and work of Norbert Wiener. This installment describes the use of software for studying the control literature by exploring collaborations between researchers. An example application draws connections between Norbert Wiener, Hendrik Bode, and other renowned researchers.

In "Conference Reports," Lucy Pao and Daniel Abramovich report on the 2013 American Control Conference that was held on June 17–19 in Washington, D.C., and Panos Antsaklis and Kimon Valavanis report on the 2013 Mediterranean Conference on Control and Automation that took place in Platanias-Chania, Crete, on June 25–28. In "ACC Preview," Dawn Tilbury provides a preview of the American Control Conference that will held on June 4–6, 2014 in Portland, Oregon.

Among the regular columns, "25 Years Ago" revisits an article by Jean-Jacques E. Slotine on the importance of incorporating physical considerations into the design of control systems. "Conference Calendar" lists upcoming conferences sponsored or cosponsored by the CSS over the next three years. "Book Announcements" provides summaries of recently published books in the control field. "Lighter Side" considers the role of control in driving in poor weather conditions. "Random Inputs" reconsiders the design of feedback control systems to teach students about feedback control systems.

REFERENCES

[1] M. Ezzeldin, P. P. J. van den Bosch, and S. Weiland, "Toward better printing quality for a drop-on-demand ink-jet printer: Improving performance by minimizing variations in drop properties," *IEEE Control Syst. Mag.*, vol. 33, no. 1, pp. 42–60, Feb. 2013.

[2] Z. W. Ulissi, M. S. Strano, and R. D. Braatz, "Control of nano and microchemical systems," *Comput. Chem. Eng.*, vol. 51, no. SI, pp. 149–156, 2013.

[3] S. V. Karnik, M. K. Hatalis, and M. V. Kothare, "Towards a palladium micro-membrane for the water gas shift reaction: Microfabrication approach and hydrogen purification results," *J. Microelectromech. Syst.*, vol. 12, no. 1, pp. 93–100, Feb. 2003.

[4] B. Borovic, F. L. Lewis, W. McCulley, A. Q. Liu, E. S. Kolesar, and D. O. Popa, "Control issues for microelectromechanical systems," *IEEE Control Syst. Mag.*, vol. 26, no. 2, pp. 18–21, Apr. 2006.

[5] Z. W. Ulissi, M. C. Molaro, M. S. Strano, and R. D. Braatz, "Systems nanotechnology: Identification, estimation, and control of nanoscale systems," in *Proc. American Control Conf.*, Montreal, QC, June 2012, pp. 1–7.

[6] M. V. Kothare, "Dynamics and control of integrated microchemical systems with application to micro-scale fuel processing," *Comput. Chem. Eng.*, vol. 30, nos. 10–12, pp. 1725–1734, 2006.

[7] R. Probst, Z. Cummins, C. Ropp, E. Waks, and B. Shapiro, "Flow control of small objects on chip: Manipulating live cells, quantum dots, and nanowires," *IEEE Control Syst. Mag.*, vol. 32, no. 2, pp. 26–53, Apr. 2012.

[8] A. Nacev, R. Probst, S. H. Kim, A. Komaee, A. Sarwar, R. Lee, D. Depireux, M. Emmert-Buck, and B. Shapiro, "Towards control of magnetic fluids in patients: Directing therapeutic nanoparticles to disease locations," *IEEE Control Syst. Mag.*, vol. 32, no. 3, pp. 32–74, June 2012.

[9] A. Sebastian, A. Pantazi, H. Pozidis, and E. Eleftheriou, "Nanopositioning for probe-based data storage," *IEEE Control Syst. Mag.*, vol. 28, no. 4, pp. 26–35, Aug. 2008.

[10] H. Butler, "Position control in lithographic equipment: An enabler for current-day chip manufacturing," *IEEE Control Syst. Mag.*, vol. 31, no. 5, pp. 28–47, Oct. 2011.

[11] R. B. Wiener and W. A. Cebuhar, "Nonlinear compensation for pneumatic actuators with hysteresis—Precision motion control for microlithography," *IEEE Control Syst. Mag.*, vol. 25, no. 6, pp. 32–44, Dec. 2005.

[12] S. O. R. Moheimani, "Invited review article: Accurate and fast nanopositioning with piezoelectric tube scanners: Emerging trends and future challenges," *Rev. Sci. Instrum.*, vol. 79, no. 7, Article. 071101, pp. 1–11, 2008.

[13] M. Srinivasa, S. Salapaka, and M. V. Salapaka, "Scanning probe microscopy," *IEEE Control Syst. Mag.*, vol. 28, no. 2, pp. 65–83, Apr. 2008.

[14] R. D. Braatz, R. C. Alkire, E. G. Seebauer, E. Rusli, R. Gunawan, T. O. Drews, and Y. He, "Perspectives on the design and control of multiscale systems," *J. Process Control*, vol. 16, no. 3, pp. 193–204, 2006.

Richard D. Braatz

The Healing Power of Feedback …

This is extremely fortunate for it means that a feedback chosen to stabilize the infinitesimal approximation also stabilizes the original nonlinear system and greatly improves the accuracy of the approximation. This is the fundamental mathematical fact that allows one to use linear models obtained by infinitesimal approximation (after being stabilized by feedback) to model nonlinear processes in the small.

—Arthur J. Krener, Alberto Isidori, and Witold Respondek, "Partial and robust linearization by feedback," *Proceedings of the 22nd IEEE Conference on Decision and Control*, San Antonio, Texas, December 14–16, 1983, pp. 126–130.

YINGFENG SHAN
and KAM K. LEANG

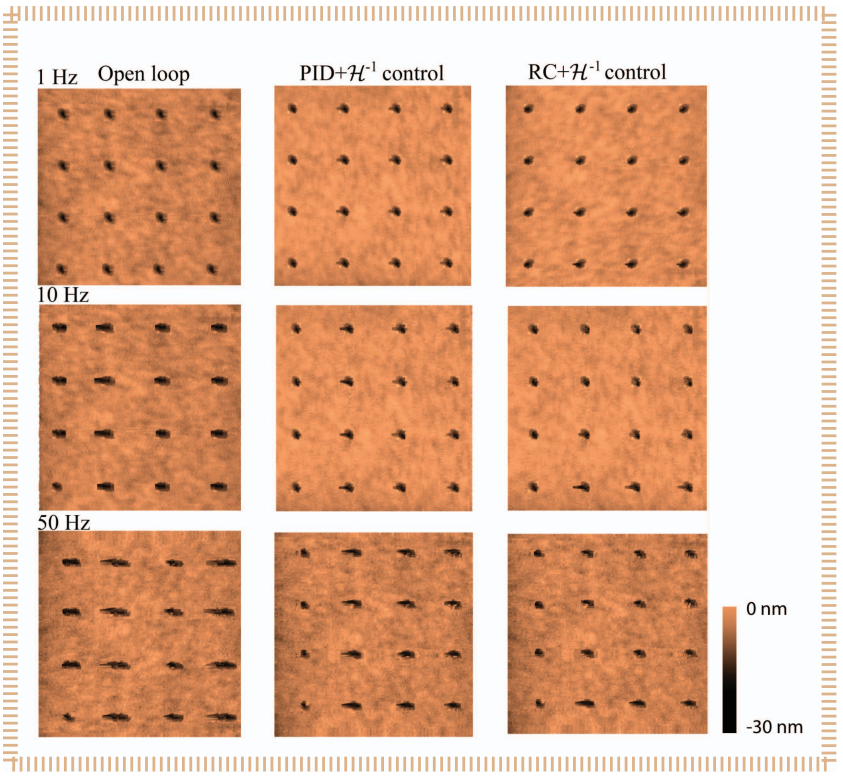

Design and Control for High-Speed Nanopositioning

SERIAL-KINEMATIC NANOPOSITIONERS AND REPETITIVE CONTROL FOR NANOFABRICATION

This article focuses on the design and control of nanopositioning systems (nanopositioners) that operate mostly in a repetitive fashion. In addition to accuracy, speed is also a crucial requirement for these systems. Multi-axis nanopositioners are critical in applications such as atomic force microscopy (AFM) [1], fiber optic alignment [2], micro- and nanomachining [3], [4], and nanometrology [5], [6]. More specifically, for video-rate scanning probe microscopy (SPM) and high-throughput probe-based nanofabrication [7], the desired motion trajectory of the nanopositioner repeats from one operating cycle to the next and the motion should be as fast and accurate as possible. However, vibrations caused by mechanical resonance are a major factor limiting the speed. Typically, the bandwidth of these systems is limited by the first mode of vibration [8], [9].

Current research to improve the speed and accuracy of nanopositioning systems focuses on mechanical and control system design. Recent trends in mechanical design have favored the use of compliant mechanisms such as flexures for guiding the motion of sample stages, while at the same time the flexures are optimized to ensure the highest possible mechanical resonances [10]–[12]. With compact and stiff piezoelectric actuators as the primary mechanism for actuation, it is not uncommon for

Digital Object Identifier 10.1109/MCS.2013.2279474
Date of publication: 14 November 2013

1066-033X/13/$31.00©2013IEEE

Scanning Probe Microscopy

In scanning probe microscopy (SPM), a multi-axis nanopositioning stage is used to position a small probe relative to a specimen for nanoscale imaging, surface modification, and/or interrogation [1], [28]. Unlike a traditional optical microscope, which uses light for imaging, in SPM an image is formed by rastering a small microcantilever probe over a sample surface and plotting the probe's interaction as a function of its lateral position [78]. For example, consider one type of SPM, the atomic force microscope shown in Figure S1. This instrument is one of the most versatile applications of SPM because of its ability to work with conducting and nonconducting samples, as well as operate in a vacuum, air, or in water. In AFM, a micromachined cantilever with a sharp probe tip on its lower surface is positioned relative to a sample surface. When the probe tip is rastered over a sample's surface, tip-to-sample interaction causes the cantilever to deflect vertically with respect to the sample topology. The deflection is measured by laser and used to construct an image of the sample surface. In this case, the AFM essentially "feels" the surface with a tiny, finger-like cantilever. An AFM can generate topographical images of atoms as well as control, manipulate, and alter the properties of matter at the nanoscale [28].

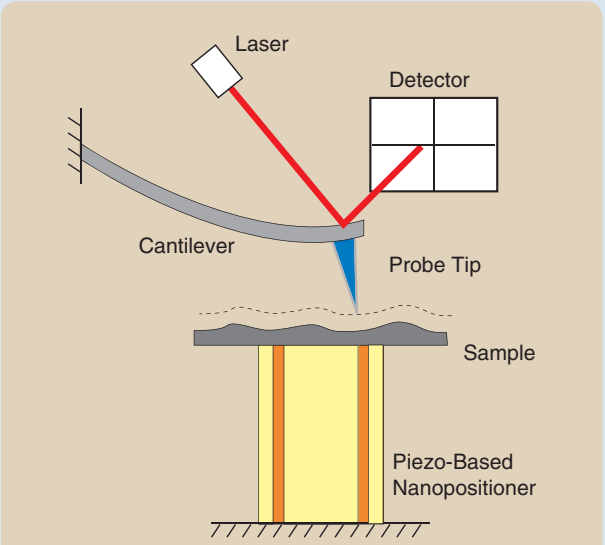

FIGURE S1 A schematic of an atomic force microscope, a type of scanning probe microscope.

Positioning the SPM probe tip relative to the sample is achieved with two basic configurations as shown in Figure S2: (a) scan by sample or (b) scan by probe. In the scan-by-sample configuration, the nanopositioner, such as the flexure-based design shown equipped with three piezo stacks, moves the sample relative to a fixed SPM probe. The x and y axis piezos position the sample in the lateral direction (parallel to the sample surface) and a z axis stack moves the sample vertically. The deflection of the cantilever is measured optically by reflecting a laser beam off the end of the cantilever onto a nearby photodetector. In the scan-by-probe arrangement [Figure S2(b)], a nanopositioner, such as the sectored tube-shaped piezoactuator, is used to move the probe laterally and vertically relative to a fixed sample. In a scan-by-probe system, typically the laser and photodector are required to move with the cantilever. However, this conjoined motion can be avoided by incorporating sensing elements into the cantilever itself, such as using piezoresistive, piezoelectric, or capacitive elements. The mechanical resonances of scan-by-sample systems are higher compared to the scan-by-probe systems due to the fact that more mass is being displaced in the latter configuration. Detailed reviews of SPM and AFM can be found in [14], [15], and [28].

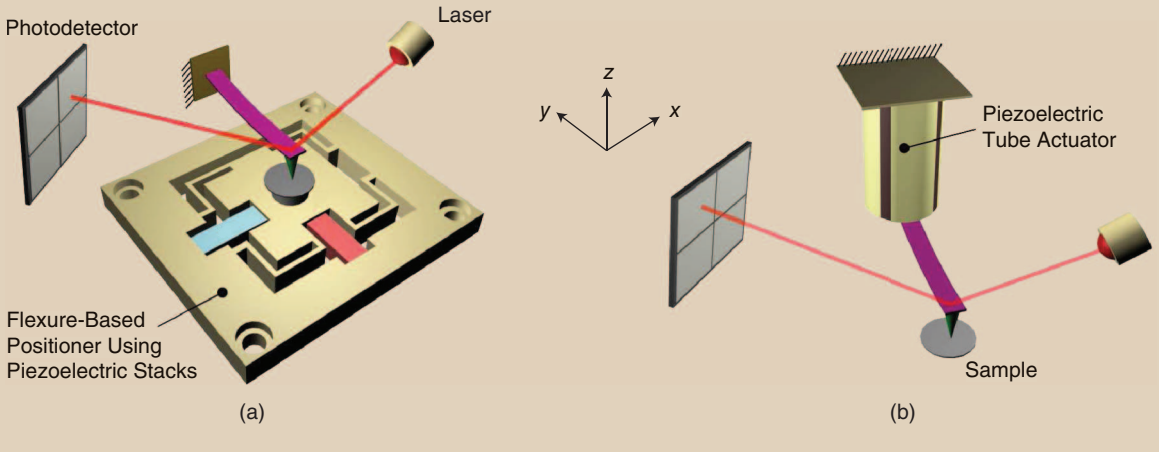

FIGURE S2 Two positioning schemes for scanning probe microscopes: (a) scan by sample and (b) scan by probe.

Serial Versus Parallel Kinematic Nanopositioners

For multi-axis nanopositioning, both serial- and parallel-kinematic mechanical designs (Figure S3) are widely employed. The effective stiffness of the actuator along the x and y direction is modeled by k_x and k_y, respectively. The effective damping of the structure in each direction is omitted for brevity, but usually it appears in parallel with each spring element. The advantages of a parallel-kinematic configuration are that runout is easily measured and corrected for [79], [80], and if both axes have the same mechanical bandwidth, the scan direction can be chosen arbitrarily [51]. However, for raster-type scanning, motion along one axis is considerably faster than the other. For example, to acquire an $n \times n$-pixel image in SPM, motion along the x-axis is n-times faster than the y-axis. For this reason, a serial-kinematic design with one high-speed stage is sufficient and may be more cost effective to design and manufacture. Particularly, only the high-speed axis requires a costly high-bandwidth, high-power piezo-amplifier. Recently, serial-kinematic nanopositioners have been considered for high-speed SPM applications [7], [52], [81]. One disadvantage, however, is the inability to measure (and correct for) parasitic motion such as runout or guiding error. Instead, low runout is achievable with properly designed flexures and mechanisms for guiding the motion of the sample stage [12].

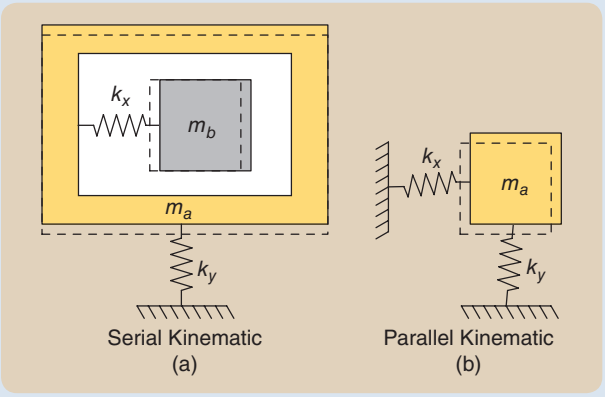

FIGURE S3 Lumped parameter models of both serial- and parallel-kinematic configurations for nanopositioners. (a) A serial-kinematic system constructed by nesting one flexure-guided mechanism. The x-axis, which is the horizontal axis in this schematic, is the fast axis in this design. (b) A parallel-kinematic system where all actuators are relative to ground. The fast axis can be either the x- or y-axis.

nanopositioning stages to have resonances in the tens of kilohertz range, making video-rate AFM imaging possible [7], [12], [13]. Feedback and model-based feedforward control schemes have been developed and implemented to dramatically improve the bandwidth and precision of a wide variety of nanopositioning platforms [9], [14]–[16]. Feedback control schemes include traditional proportional-integral (PI) or PI-derivative (PID) [17], state feedback [3], gain scheduling [18], H_∞ control [19], [20], positive position feedback (PPF) control [21], [22], and integral resonant control (IRC) [23], to name a few. Examples of model-based feedforward techniques include system inversion [8], [15], input shaping techniques [24], and iterative control algorithms [15], [25], [16].

This article looks at the problem of precision positioning for systems that operate in a periodic fashion, such as the raster-type scanning motion of nanopositioners in SPM systems (see "Scanning Probe Microscopy") [1], [28]. In many applications, nanopositioners are required to track a periodic reference trajectory, for example, in AFM, a nanopositioner is used to precisely position a tool tip relative to a sample surface in a repetitive fashion (raster scanning) to obtain information for creating high-resolution topographical images or investigate nanoscale dynamic interactions in real time [7], [27], [28]. Optimizing the mechanical design and the controller to track desired trajectories that are periodic in time is critical.

This article first discusses the key mechanical characteristics of serial-kinematic nanopositioners designed for raster-scanning type motions. In a two-axis, serial-kinematic nanopositioner, one axis is designed for high-speed positioning while the other axis exhibits considerably lower mechanical resonance for slow movements. This configuration resembles dual-stage positioners used in hard-disk drives [29], [30] as well as dual-stage atomic force microscopes [31], [32]. In this case, the mechanical design is decoupled, and each axis can be optimized for a given range, scan speed, and even precision. Designs for two high-performance serial-kinematic nanopositioning stages are presented as examples. The stages incorporate vertically stiff flexures for guiding the motion of the sample platform to minimize parasitic motion (runout) and off-axis effects. In this design, simple second-order transfer function models can be used to model the behavior between the applied input voltage and the displacement of the sample platform.

Next, the repetitive control (RC) approach is presented for tracking periodic reference trajectories and the controller is applied to a prototype serial-kinematic stage on a commercial atomic force microscope for nanofabrication. The control approach is well suited for serial-kinematic stages for scanning-type applications. RC is a direct application of the internal model principle [33], where a signal generator is incorporated into a feedback loop to provide high gain at the fundamental frequency of the reference trajectory and its harmonics [34], [35]. Recently, the RC approach was studied for scanning applications in piezo-based atomic force microscopes [36]. Repetitive controllers have also been used to address run-out issues in disk drive systems [37], [38] and to improve the performance of

machine tools [39], [40]. Compared to traditional PI or PID feedback controllers, where careful tuning is required and the residual tracking error persists from one operating cycle to the next, RC has the ability to reduce the error as the number of operating cycles increases. For applications in which the desired trajectory is periodic and the signal period is known a priori, a repetitive controller offers many advantages. For example, it can be incorporated into an existing feedback control loop to enhance performance for scanning applications. Also, compared to iterative learning control (ILC) [41]–[43], a control method that has been used extensively for piezo-based positioning systems [25], [26], RC does not require the initial condition to be reset to the same value at the start of each iteration trial [35], [43]. Additionally, compared to model-based feedforward approaches [15], [8], RC does not require extensive modeling of the system. Due to variations in the system dynamics, for example due to aging [44] or temperature variations [45], open-loop feedforward approaches often lack robustness. On the other hand, the feedback mechanism built into RC provides robustness to parameter variation. Finally, RC can be easily implemented digitally, and thus high-speed data acquisition and control hardware such as field-programmable gate array systems [46] can be used to take advantage of the RC structure for precision control.

MECHANICAL DESIGN FOR FAST SCANNING MOTION

Often, the effectiveness of a control system is limited by the dynamics of the system, thus good mechanical design is important. A good mechanical design ensures that the system's behavior is predictable, repeatable, and robust. As a contrasting example, out-of-plane modes often introduce undesirable resonance and antiresonance modes that can excite the system and add unwanted phase delays [12], [47], which affect closed-loop stability and bandwidth. These behaviors, at a minimum, make control system design and implementation a challenge. Additionally, modeling a well-behaved mechanical system is often less challenging compared to systems that exhibit undesirable behaviors, such as cross-coupling effects or out-of-plane modes and large nonlinearities (second-order models compared to high-order models). More detailed discussion of advanced mechanical design for precision positioning systems can be found in [48] and [49].

To illustrate the basics of the design, the two nanopositioners shown in Figure 1 are briefly described. One nanopositioner is designed specifically for high-speed short-range applications (a1) and the other for low-speed long-range applications (b1). Both stages are manufactured of 7075 series aluminum, using the wire electric discharge machining (WEDM) process to create a monolithic flexure-based

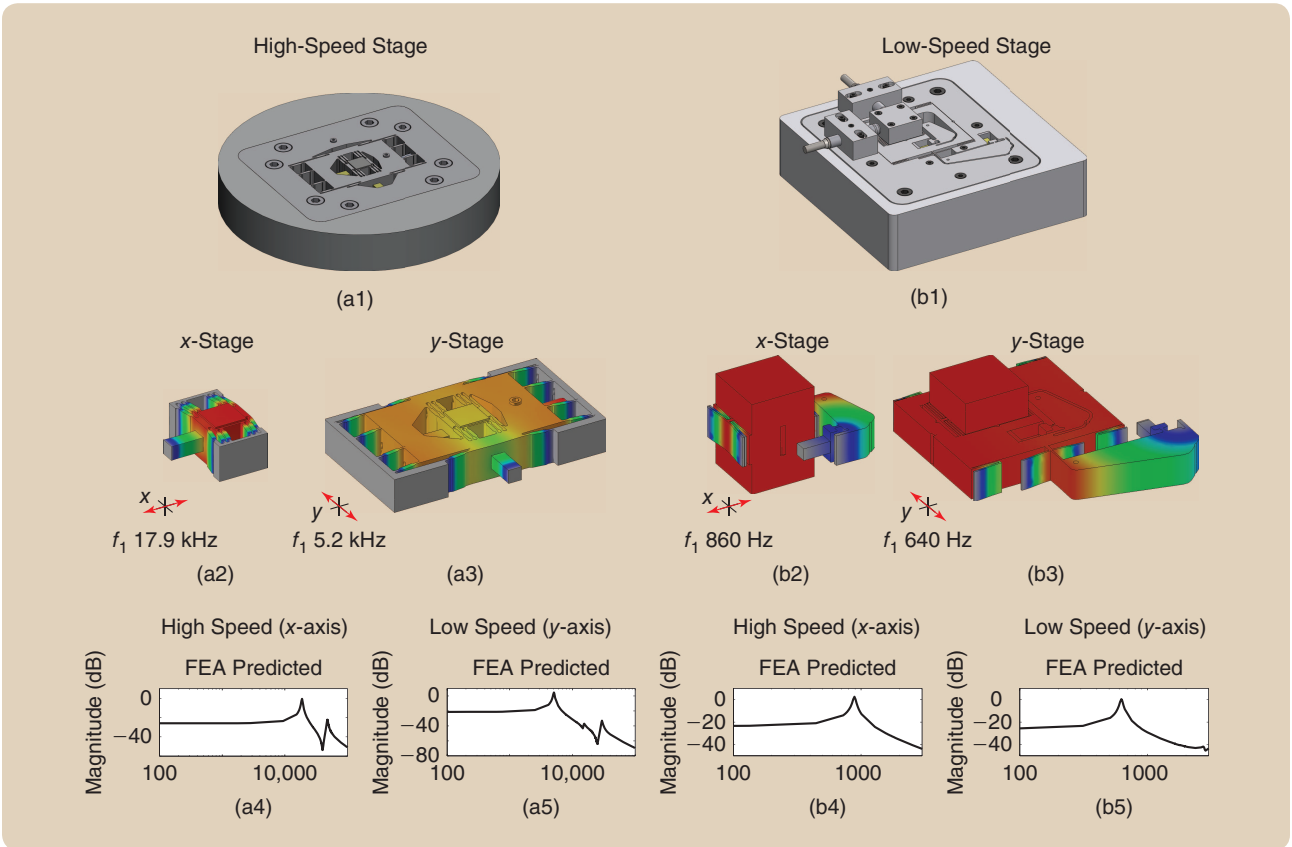

FIGURE 1 Solid model images of the (a1) high-speed and (b1) long-range nanopositioners along with FEA-predicted first resonance modes and frequency response plots for the corresponding *x*- and *y*-stages.

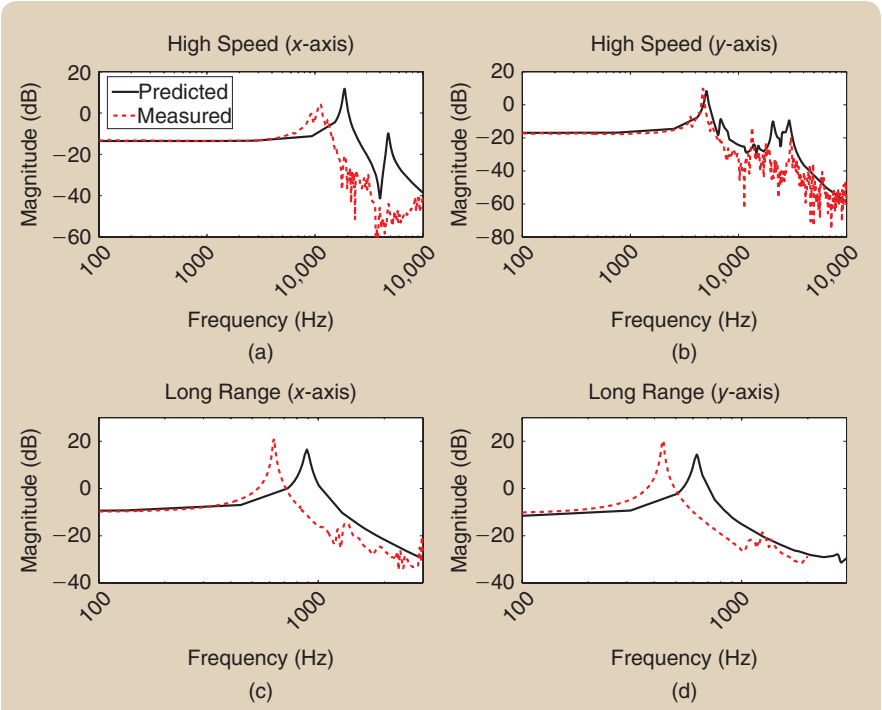

FIGURE 2 Frequency response results comparing the FEA-predicted and experimental results.

design [50]. Lateral displacements are provided by plate-stack piezoelectric actuators. Compliant flexures are used to guide the stages in their corresponding actuation directions while limiting out-of-plane (parasitic) motion and dynamic cross coupling. The stages were designed to have the actuation modes with frequencies lower than the out-of-plane modes [12], [47].

TABLE 1 Long-range static analysis.

Predicted	***x*-Stage**	***y*-Stage**
F_{in} (N)	641	641
u_{Act} (μm)	23.18	20.7
u_{Stage} (μm)	92.0	70.7
k_{Act} (N/μm)	27.0	30.97
K_{Mech} (μm/μm)	3.97	3.42
ΔL_{Po} (μm)	14.7	14.7
ΔL_{Act} (μm)	10.52	10.11
ΔL_{Stage} (μm)	41.76	34.58
Measured	***x*-stage**	***y*-stage**
ΔL_{Stage} (μm)	42.83	43.25

The high-speed stage shown in Figure 1(a1) is a three-axis serial kinematic stage designed specifically for high-speed short-range raster-scanning applications. For a discussion on serial and parallel kinematic design, see "Serial Versus Parallel Kinematic Nanopositioners." To achieve accurate positioning at high scan-rates, the stage must have very high mechanical resonance with the first mode occurring in the corresponding actuation direction [51], [52], [53]. Having the first dominant mode along the actuation direction also ensures that second-order models can be used to model the dynamics of the positioning stage. To have these dynamics, the scanning stage must have a high stiffness-to-mass ratio k/m in the actuation direction (lateral x), and even higher stiffness-to-mass (or inertia) ratios in the out-of-plane directions (vertical z, lateral y, and rotational x, y, z) [12]. Stiff actuators are used, the stage is designed to be light and compact, and compliant flexures are designed to guide the stage in the desired direction while constraining out-of-plane motion. In some cases, careful attention must be given to material deformation of the sample platform during operation to avoid cross-coupling behavior.

Plate-stack piezoelectric actuators are used because they are stiff and compact. For example, a $5 \times 5 \times 10$ mm stack piezoactuator (Noliac SCMAP07) offers approximately 10 μm of stroke and can be used to drive the lateral x- and y-stages. The actuators are used in a direct drive configuration to exploit their stiffness characteristics. In-plane and out-of-plane stiffness may be increased by using actuators with larger cross-sectional dimensions. However, a proportional increase in capacitance is observed with increased cross-sectional area, yielding an undesirable increase in power requirements. For this reason, out-of-plane stiffness is increased through flexure design and placement. The vertical stiffness of the flexures is increased by increasing the total number (quantity) of flexures, decreasing the overall flexure length, and thickening the center section of the flexure [12], [53]. Vertically stiff flexures are placed at the lateral corners of the stage to increase rotational stiffness. The stage is manufactured out of 7075 aluminum for its high elastic modulus to density ratio E/ρ (light and stiff).

Finite element analysis (FEA)(SolidWorks Simulation) was used to predict the mechanical resonance modes of the lateral x- and y-stages and their corresponding harmonic frequency responses. It is assumed that the dynamic motion

Hysteresis and Dynamic Effects in Piezo-Based Positioning Systems

A common assumption is that piezoelectric actuators expand and contract proportionally to an applied voltage. Unfortunately, this assumption is not accurate and is particularly erroneous when considering moderate or high electric fields or when the frequency of operation becomes high. There are two significant sources of error that degrade and complicate the response of piezoelectric positioners: hysteresis and dynamic effects, the latter of which includes creep and vibration, as illustrated in the measured response shown in Figure S4.

Hysteresis is a nonlinear behavior between the applied electric field and the mechanical displacement of a piezoelectric actuator, believed to be caused by irreversible losses that occur when similarly oriented electric dipoles interact upon application of an electric field [82]. The effect of hysteresis on the displacement of a piezoelectric actuator is more pronounced over large-range motion [17], [83]. In Figure S4, the curve depicts the nonlinearity that arises due to hysteresis. In addition to poor positioning accuracy, hysteresis causes poor repeatability and the mixing of harmonic content into the displacement response. Hysteresis can be avoided by operating in the linear range, that is, over short displacements, but such operation limits the achievable position. Controlling the charge delivered to the piezoelectric transducer, rather than the voltage, helps to minimize hysteresis [84].

When a piezoelectric transducer is commanded by a step change in voltage, the response consists of high-frequency transients followed by low-frequency drift known as creep. The time constant for creep is typically a few minutes. Creep severely degrades the low-frequency and static positioning ability of piezoelectric actuators [85]–[87]. In mechanics, creep is a rate-dependent plastic deformation of the material when subjected to a constant load or stress [88]. Similarly, creep in piezoelectric materials is a rate-dependent deformation due to a constant electric field. Creep manifests as remnant polarization that slowly increases after the application of a constant electrical field. One method to avoid creep is to operate fast enough so that the creep effect becomes negligible [8]. However, such fast operation prevents the use of piezo positioners in slow and static applications. For example, due to drift, precise fabrication of nanofeatures using atomic force microscopes is difficult when the process time-scale is on the order of minutes [85]. Methods to compensate for creep have been well studied in the past and some examples include the use of feedback control [17], [89], [90], [20], and model-based feedforward control [87], [91]–[94], [8].

Vibration (or actuator) dynamics, such as structural resonances, limit the operating bandwidth of piezo-based positioning systems. The effect is caused by command signals exciting the flexible modes of the structure [95], [96]. For example, the frequency response of a piezo-based positioner typically has sharp resonant peaks. These peaks are easily excited by certain command signals, such as triangular inputs applied to control the positioner. Figure S4 illustrates the effect of vibration, where oscillations cause significant tracking error in the displacement. Such effects cause distortion in SPM-based imaging, such as the rippling effect in AFM images. Typically, scan rates (that is, scan frequencies) are restricted to less than 1–10% of the first resonant frequency, thus limiting the bandwidth of piezo-based systems since the achievable scan rate is lower for increased resolution in positioning. Higher operating speed can be achieved by using *stiffer* piezoactuators with higher resonant frequencies [97], [13], [98], but stiff piezos have shorter effective displacement ranges. Therefore, the use of stiffer piezos to increase bandwidth also leads to a reduction of the positioning range.

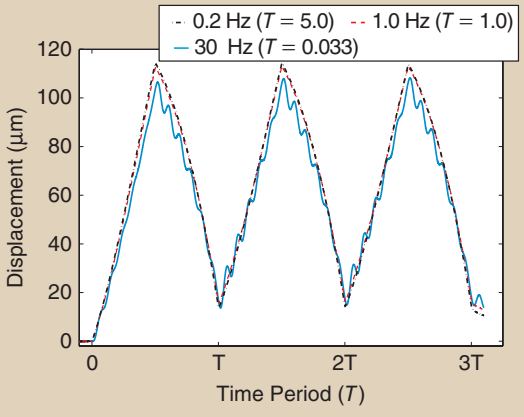

FIGURE S4 Experimentally measured response of a piezoactuator showing hysteresis, creep, and vibration effects.

of the high-speed x-stage will not excite the modes of the y-stage. For this reason, the x-stage is investigated as a separate entity. The first mechanical resonance modes for the high-speed x- and low-speed y-stages are shown in Figure 1(a2) and (a3) to occur at 17.9 kHz and 5.2 kHz, respectively, both in their corresponding actuation directions. The predicted in-plane frequency response plots for the x- and y-stages are shown in Figure 1(a4) and (a5)

The long-rage stage, shown in Figure 1(b1), couples a $5 \times 5 \times 12$ mm Noliac SCMAP07 plate stack actuator with free stroke of 14.7 μm with a mechanical displacement amplifier to provide a final stage displacement of approximately 40 μm. The stock ceramic end caps of the actuators were replaced with alumina plates to increase the actuator stiffness as described in [12]. The lever arm of the mechanical amplifier has an ideal mechanical displacement amplification of 5.82 ($K_{\text{mech}} = u_{\text{out}}/u_{\text{in}}$). It is shown later that the resultant amplification for the amplifier is just under four times, due to compliance in the lever and associated flexures. The stage bodies were guided linearly with compliant flexures. Compound flexures were attached to the corners to keep the stage compact while maintaining low actuation

The Repetitive Control Approach

Repetitive control is a direct application of the internal model principle [33], where high-accuracy tracking of a desired periodic trajectory with period T_p is achieved if the controller consists of the transfer function of the reference trajectory [34], [35], [99]. One such controller is a signal generator (Figure S5) with period T_p. The *plug-in* RC is created by wrapping a pure delay z^{-N} inside of a positive-feedback loop, where the integer $N = T_p/T_s$ is the number of points per period T_p of the reference trajectory $R(z)$ and T_s is the sampling time. In the block diagram, $G_c(z)$ is a feedback controller, such as an existing proportional-integral-derivative (PID) controller. A low-pass filter $Q(z)$ is inserted to lower the high gain of the RC at high frequencies to ensure stability and robustness [100], [37]. A tradeoff is made between robustness and high-frequency tracking when such filters are used.

In the absence of the low-pass filter $Q(z)$, the poles of the signal generator are $1 - z^{-N} = 0$, which implies infinite gain at the harmonics of the periodic reference trajectory ($\omega = 2n\pi/T_p$, where $n = 1, 2, 3, \ldots$), as shown in Figure S6. Such large gain is what gives the RC its ability to track periodic trajectories. Practical RC design incorporates a low-pass filter $Q(z)$ because the large gain at high frequencies can lead to instability of the closed-loop system.

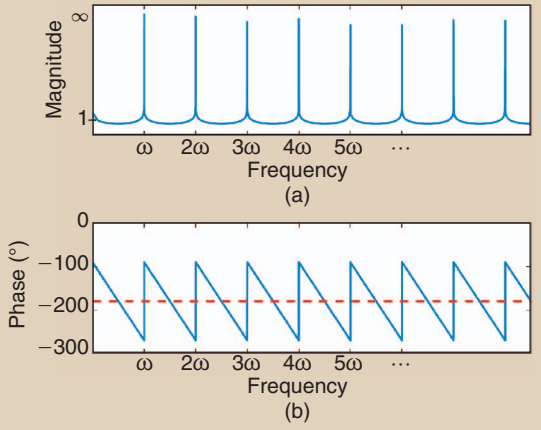

FIGURE S6 Magnitude and phase as a function of frequency for signal generator $z^{-N}/(1 - z^{-N})$, where $z = e^{j\omega T_s}$.

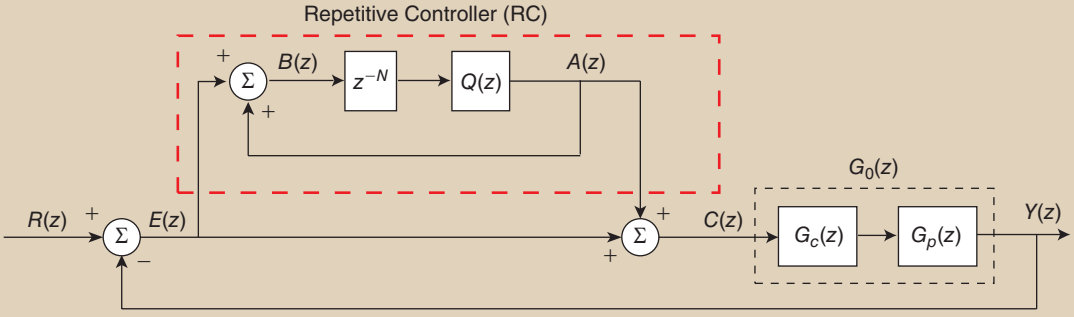

FIGURE S5 A repetitive control feedback system.

stiffness. Beam flexures were added to the fore and aft ends of the stage bodies to increase rotational stiffness, thus reducing the effects of parasitic motion and dynamic cross coupling. Parabolic fillets were used instead of constant radius corner fillets in areas subject to high strain to decrease the stress concentration. The final stage displacement was determined to be 41.76 µm and 34.58 µm for the x- and y-axes as shown in Table 1. The first mechanical resonance modes for the x- and y-stages are shown in Figure 1(b2) and (b3) to occur at 860 Hz and 640 Hz, respectively, both in their corresponding actuation directions. The predicted in-plane frequency response plots for the x- and y-stages are shown in Figure 1(b4) and (b5).

TABLE 2 Comparison of dominant resonance modes.

	High-Speed x	High-Speed y	Long-Range x	Long-Range y
Predicted	17.9 kHz	5.20 kHz	860 Hz	640 Hz
Measured	11.1 kHz	4.68 kHz	627 Hz	439 Hz
Difference*	38%	10%	27%	31%

*(Predicted – Measured)/Predicted × 100

The mechanical performance of the nanopositioning stages was determined experimentally. The high-speed stage was outfitted with inductive sensors (Kaman SMU9000-15N) to measure displacement in the lateral directions and the capacitive sensors (ADE 5300 sensor with 5501 module)

were used on the long-range stage. The lateral (x/y) range of motion was determined to be 10×10 μm for the high-speed stage and 42.83×43.25 μm for the long-range stage. Frequency response was measured using a dynamic signal analyzer (Stanford Research Systems SRT785). Small inputs (<70 mV) were applied to the piezo amplifiers and measurements for the x- and y-stages were taken with the stage-mounted sensors. In-plane frequency response results for the high-speed and long-range stages are shown in Figure 2(a)–(d). The results show that the dominant resonance modes for the x- and y-stages for both the high-speed scanner and long-range stage are second order as predicted by FEA. The FEA-predicted and measured values of the dominant resonance modes are compared in Table 2. The measured results are 10–38% lower than the predicted values, which is likely due to nonideal connections in the assembly, nonideal boundary conditions, and insufficient piezoactuator preload.

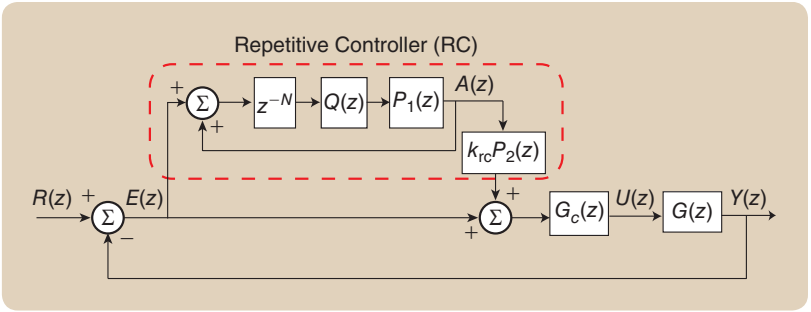

FIGURE 3 The block diagram of a plug-in repetitive-control system consisting of two linear phase-lead compensators, $P_1(z)$ and $P_2(z)$, to enhance performance.

TRACKING PERIODIC TRAJECTORIES: REPETITIVE CONTROL (RC) APPROACH

Many applications in nanopositioning require the positioning system to execute a scanning-type motion, which is often periodic in time. RC is well suited for tracking periodic motion trajectories, where the objective of the control problem is to achieve high-precision positioning. This objective is achieved by adding RC to an existing closed-loop feedback system (such as a PID feedback controller) to improve performance.

This section first presents the RC concept and a basic RC system is described for SPM application. Next, a more advanced dual-RC is presented for improved performance, followed by design approaches to deal with the hysteresis nonlinearity that is common in piezo-based nanopostioners.

Challenges and Motivation

Nanopositioning systems exhibit hysteresis and dynamic effects (vibration and creep) and these behaviors are often challenging to control [9], [14]. For more details about hysteresis and dynamic effects, and a brief survey of existing control methods to handle these behaviors, see "Hysteresis and Dynamic Effects in Piezo-Based Positioning Systems." Particularly, hysteresis can lead to significant tracking error, approximately 20% in piezo-based positioners [54]. Without compensation, hysteresis can affect the stability and tracking performance of a closed-loop controller, especially when the controller is designed around a linear dynamic model [55]. While hysteresis is typically regarded as a range-dependent effect, dynamics (vibration and creep), on the other hand, depend on the input frequency. For example, the structural vibrations in piezoactuators become significant when the input frequency approaches the dominant resonant frequency, where high frequency inputs excite lightly damped structural modes causing severe oscillations in the output response. The total tracking error can exceed 30% [54], and therefore hysteresis and dynamic effects limit both the range as well as the bandwidth of operation. This is especially true in AFM applications where hysteresis and dynamics dominate the response of the piezo-based positioning system, preventing the tool from precisely tracking a desired motion trajectory, such as the scanning trajectory for AFM imaging or probe-based nanofabrication [9], [15]. Moreover, the large tracking error causes the scanning probe microscope probe tip to experience large tip-to-sample forces that can damage, for example, the scanning probe microscope probe or soft specimens such as live cells. Precision positioning of the scanning probe microscope tool tip relative to a sample surface is needed to obtain high-resolution topographical images, measure various properties of a specimen, and investigate nanoscale dynamic interactions in real time [7], [28]. Therefore, control of hysteresis and dynamic effects is critical in nanopositioning systems.

Enhanced Plug-in RC for Nanopositioning

Periodic motion trajectories are common in nanopositioning applications, for example, the raster pattern is used in SPM for imaging [14]. By exploiting the process of repetition, RC

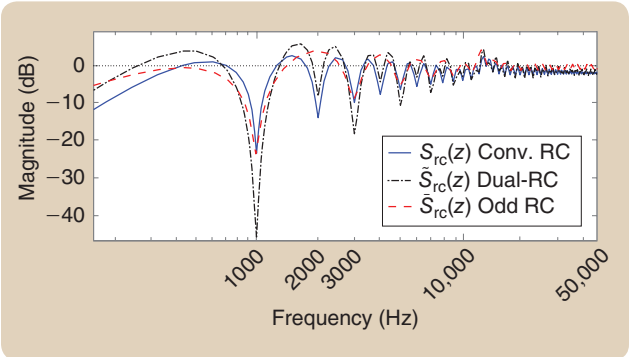

FIGURE 4 Comparison of magnitude versus frequency plots for the sensitivity functions for different repetitive-control (RC) configurations, where $S_{rc}(z)$ denotes conventional RC (solid line), $\bar{S}_{rc}(z)$ represents dual RC (dash-dot line), and $\tilde{S}_{rc}(z)$ is for odd-harmonic RC (dashed line).

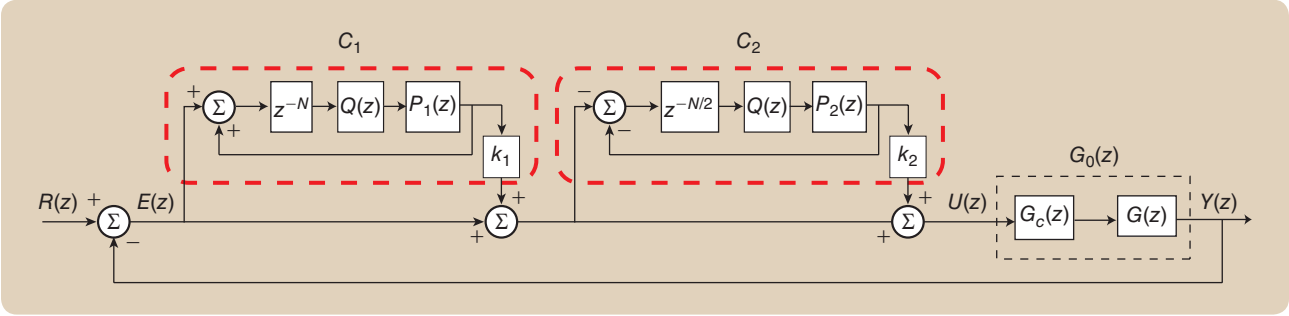

FIGURE 5 A dual-stage repetitive-control design consisting of a conventional RC (C_1) cascaded with an odd-harmonic RC (C_2).

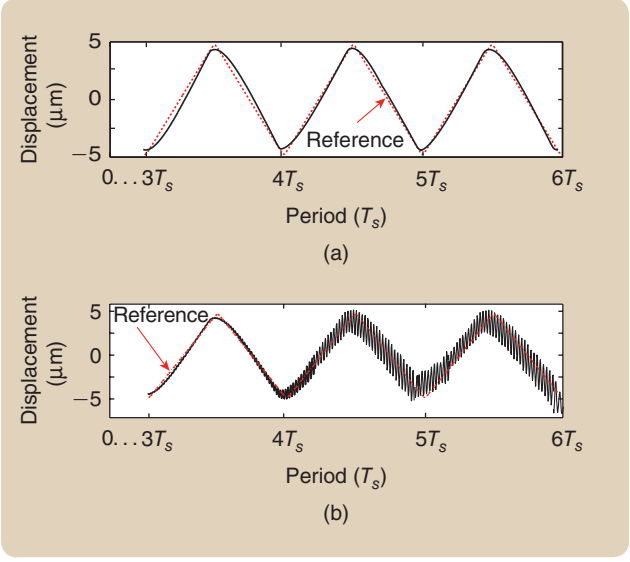

FIGURE 6 (a) Simulation and (b) experimental results showing the effect of hysteresis on closed-loop system stability and tracking performance.

has recently been considered for precision tracking of scanning-type motion nanopositioning systems [36]. The RC approach is based on the internal model principle [33] and is specifically designed to track periodic reference trajectories; see "The Repetitive Control Approach" for a discussion of the basic features of RC and key challenges. A repetitive controller consists of a signal generator that provides high gain at the harmonics of the reference trajectory. The controller is often implemented digitally using a pure delay inside of a positive feedback loop [34], although analog implementations have been proposed [56], [57]. Compared to traditional feedback and feedforward controllers, the tracking error of RC diminishes as the number of operating periods increases. The controller generally requires only the period of the reference trajectory to be known [34]. In many motion control applications, such as SPM-based imaging and patterning, the reference signal's period is known in advance, which makes RC attractive. For convenience, RC can be incorporated into an existing feedback loop to track periodic signals and disabled when not needed. For improved performance, an RC can be combined with feedback controllers such as damping controllers [21], [22], [58] to suppress the effects of sharp resonances.

A discrete-time repetitive controller designed for a linear dynamic model of the piezoactuator is shown in Figure 3, where $R(z)$ is a periodic reference trajectory with period T_p, k_{rc} is the RC gain, T_s is the sampling period, $N = T_p/T_s$ is an integer number that represents the number of points per period of the reference trajectory, and two positive phase-lead compensators, $P_{1,2}(z) = z^{m_{1,2}}$, where m_1, m_2 are nonnegative integers, are added to improve tracking performance [36]. Notably, $P_1(z)$ compensates for the phase lag of the low-pass filter $Q(z)$ while $P_2(z)$ compensates for the phase lag of the closed-loop system. It is emphasized that both phase-lead compensators contribute a linear phase lead angle of

$$\theta_i(\omega) = m_i T_s \omega, \quad i = 1, 2 \tag{1}$$

in units of radians. A typical feedback controller, such as a PID, is represented by $G_c(z)$, and it is assumed that the feedback controller is part of the forward path and designed such that the closed-loop system without the RC would be asymptotically stable.

The design of the RC is accomplished by properly choosing the RC gain k_{rc}, along with the values of m_1 and m_2 for the phase-lead compensators $P_1(z)$ and $P_2(z)$. The objective is to find a balance between the tracking performance and the stability of the RC closed-loop system.

Let $T(z)$ represent the complimentary sensitive function of the closed-loop feedback system without RC, that is, $T(z) = G_0(z)S(z)$, where $G_0(z) = G_c(z)G(z)$ and $S(z) = 1/(1 + G_0(z))$ is the sensitivity function of the feedback system without the repetitive controller. By noting that $|Q(e^{j\omega T_s})| \le 1$ and replacing the complimentary sensitive function of the closed-loop system without RC with

$$T(e^{j\omega T_s}) = G_0(e^{j\omega T_s})S(e^{j\omega T_s}) = \frac{G_0(e^{j\omega T_s})}{1 + G_0(e^{j\omega T_s})} = |A(\omega)|e^{j\theta_T(\omega)}, \tag{2}$$

where $|A(\omega)| > 0$ and $\theta_T(\omega)$ are the magnitude and phase of $T(e^{j\omega T_s})$. Applying the small gain theorem shows that the closed-loop system is stable provided that [36]

$$0 < k_{rc} < \frac{2\cos[\theta_T(\omega)+\theta_2(\omega)]}{|A(\omega)|} \quad (3)$$

and

$$-\pi/2 < \theta_T(\omega)+\theta_2(\omega) < \pi/2. \quad (4)$$

Several observations are noted. First, the RC gain k_{rc} and the phase lead $\theta_2(\omega)$ affect the stability of the feedback-controlled system as shown in (3)–(4). Additionally, the value of the RC gain k_{rc} controls the rate of convergence of the tracking error. Because $N \gg m_1$, the modified delay z^{-N+m_1} is causal and can be implemented digitally. Finally, the tracking performance will, in some sense, be limited by the low-pass filter $Q(z)$. Specifically, the filter $Q(z)$ reduces the gain of the repetitive controller. Below, a dual-stage RC system is discussed to further improve the tracking performance.

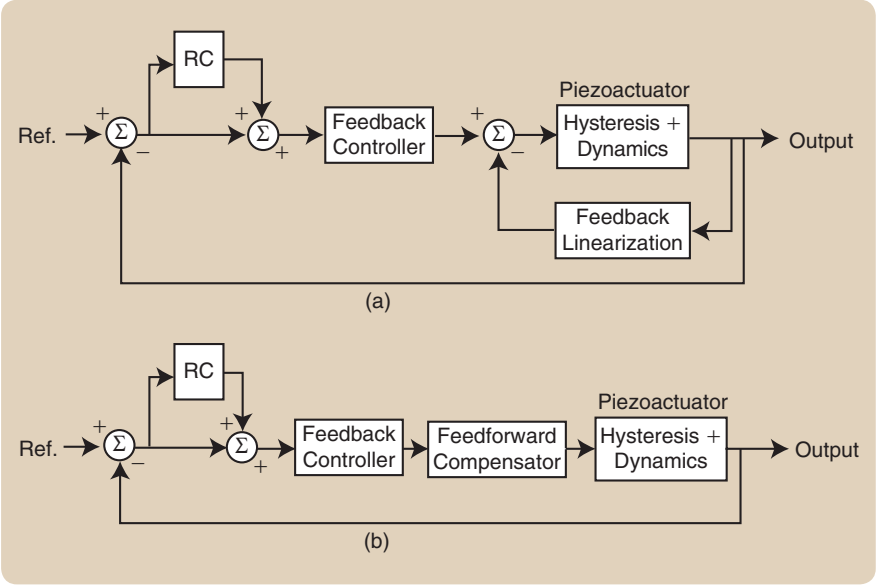

FIGURE 7 Techniques to account for hysteresis in repetitive-control design: (a) feedback-linearization approach and (b) feedforward hysteresis compensation [64].

Dual-Stage RC

Although the RC system described above is effective for tracking periodic trajectories in piezo-based nanopositioning systems [36], [12], the tracking performance is limited by the low-pass filter $Q(z)$ [59]. To further improve the performance of the repetitive controller, a high-performance dual-stage repetitive controller (dual-RC) is designed. Specifically, a discrete-time, dual-RC is created by cascading the aforementioned repetitive controller with an odd-harmonic repetitive controller. The gain characteristics of this dual-RC and the odd harmonics of the scanning-type periodic reference trajectory align and the new controller structure offers lower tracking error compared to a single RC.

The tracking performance of the RC system shown in Figure 3 is governed by the sensitivity function

$$S_{rc}(z) \triangleq \frac{E(z)}{R(z)} = \frac{[1-H_1(z)]S(z)}{1-H_1(z)[1-k_{rc}P_2(z)G_0(z)S(z)]}, \quad (5)$$

where $H_1(z) = Q(z)z^{-N+m_1}$. The magnitude response of the sensitivity function S_{rc} is shown in Figure 4 by a solid line. The frequency response function is generated in Matlab using the '`margin`' command with $N = 100$, $m_1 = m_2 = 0$, $Q(z) = 1$, and $T_s = 10$ μs as an illustrative example.

To improve the tracking performance, the magnitude of S_{rc} is reduced by cascading two signal generators together, essentially producing a squaring effect [60]. However, since the majority of reference trajectories used in scanning-type applications are odd-harmonic signals (such as triangle signals), it is preferred to cascade the basic RC, labeled C_1, with the odd-harmonic repetitive controller C_2 (Figure 5). The resulting sensitivity function is

$$\overline{S}_{rc}(z) = \frac{[1-H_1(z)][1-H_2(z)]}{W(z)+[1-H_1(z)(1-k_1)][1-H_2(z)(1-k_2)]G_0(z)}, \quad (6)$$

where $W(z) = [1-H_1(z)][1-H_2(z)]$ and $H_2(z) = -z^{-N/2+m_2}Q(z)$. The magnitude response of the sensitivity function $\overline{S}_{rc}$ is shown in Figure 4, dash-dot line (where $N = 100$, $m_1 = m_2 = 0$, $Q(z) = 1$, and $T_s = 10$ μs).

For comparison, the sensitivity function $\overline{S}_{rc}(z)$ of the odd-harmonic RC represented by C_2 in Figure 5 is

$$\overline{S}_{rc}(z) = \frac{[1-H_2(z)]S(z)}{1-H_2(z)[1-k_2G_0(z)S(z)]}. \quad (7)$$

The magnitude response of the sensitivity function $\overline{S}_{rc}$ is shown in the dashed line in Figure 4.

A comparison of the three RC configurations in Figure 4 shows that the odd-harmonic repetitive controller has less effect on the even harmonics than conventional RC (gain at first even harmonic (2000 Hz): −13.7 dB for conventional RC, 4.49 dB for odd-harmonic RC, and −8.69 dB for dual-RC). However, the magnitude of the sensitivity function for dual-RC is significantly lower than conventional RC at the odd-harmonics (−24.4 dB for conventional RC versus −47.1 dB for dual-RC at the first odd harmonic). This implies that 1) the odd-harmonic RC has the same tracking performance as conventional RC for tracking odd-harmonic trajectories but it provides the system with more robustness by reducing the gain at the even harmonics, which effectively minimizes

Prandtl-Ishlinskii Model for Hysteresis

The Prandtl-Ishlinskii (P-I) model is an operator-type model that has recently been investigated to model hysteresis in piezoactuators [70], [71], [101]. In this model, the output is characterized by the *play operator* shown in Figure S7 [70]. Let the input u be continuous and monotone over the interval $t_i \in T_i \triangleq [t_i, t_{i+n}]$, for $n = 1, 2, \cdots, N$. The play operator $\mathcal{P}_r$ is defined as

$$\mathcal{P}_r[u](0) = p_r(f(0), 0) = 0, \tag{S1}$$
$$\mathcal{P}_r[u](t) = p_r(f(t), p_r[f](t_i)), \tag{S2}$$

where

$$p_r(f(t), p_r[f](t_i)) = \max(f - r, \min(f + r, p_r[f](t_{i-1}))),$$

$f(t) = g_0 u(t) + g_1$ (with g_0, g_1 constant), and $u(t)$ is the input. The play operator's threshold is denoted by r and three examples are shown in Figure S7(a). The output $v(t)$ is a weighted sum of play operators,

$$v(t) = \mathcal{H}[u](t) \triangleq kf(t) + \int_0^R d(r)\mathcal{P}_r[u](t)\,dr, \tag{S3}$$

where k is a positive constant and $d(r)$ is a density function that affects the shape and size of the hysteresis curve. An example hysteresis curve generated from the P-I model for a piezoactuator is shown in Figure S7(b). Compared to the Preisach hysteresis model, the P-I model is less computationally demanding to implement and invert for feedforward control.

An inverse of the P-I model is proposed based on the observation of the shape of the input versus output curve shown in Figure S8(a). For such a curve, the inverse-play-type operator shown in Figure S6(b) is proposed for constructing the inverse model.

Therefore, the inverse-play operator shown in Figure S8(b) is described by

$$\mathcal{P}_{\text{inv},r'}[v](0) = p_{\text{inv},r'}(h(0), 0) = 0,$$
$$\mathcal{P}_{\text{inv},r'}[v](t) = p_{\text{inv},r'}(h(t_i), \mathcal{P}_{\text{inv},r'}[h](t_i)), \tag{S4}$$

where $p_{\text{inv},r'}(h(t), p_{\text{inv},r'}[h](t_i)) = \max(-h - r', \min(-h + r', p_{\text{inv},r'}[h](t_{i-1})))$ and r' denotes the threshold of the inverse-play operator. Then, the output of the inverse hysteresis model is

$$\mathcal{H}^{-1}[v](t) \triangleq k_{\text{inv}} h(t) + \int_0^R d_{\text{inv}}(r')\mathcal{P}_{\text{inv},r'}[v](t)\,dr'. \tag{S5}$$

The function $h(t) = g_0' v(t) + g_1'$, where $v(t)$ is the output of the hysteresis behavior and g_0', g_1' are constants.

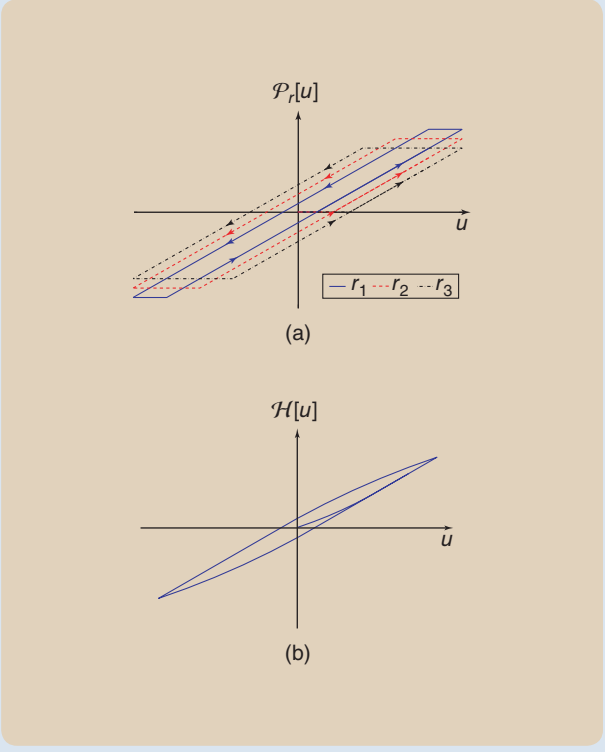

FIGURE S7 (a) The play operator with threshold r. (b) The output of the Prandtl-Ishlinskii hysteresis model for a piezoactuator.

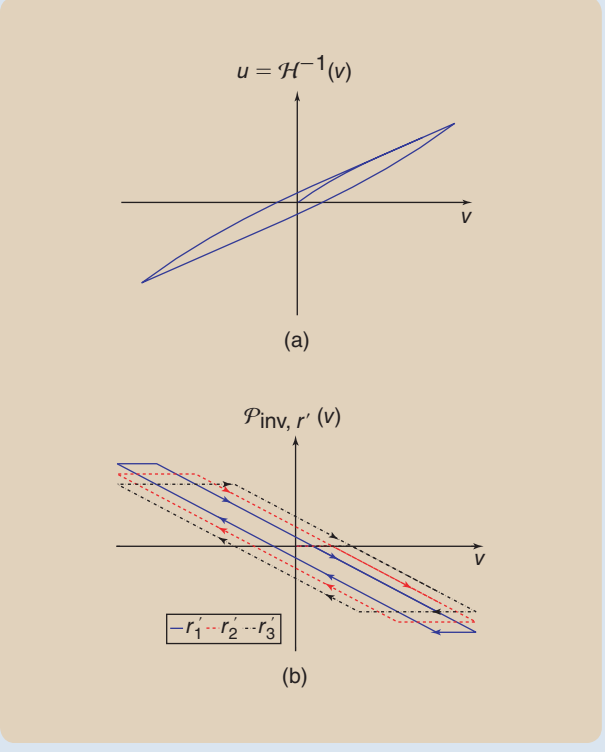

FIGURE S8 (a) Input versus measured output plot. (b) A play-type operator for the inverse model with threshold r'.

the amplification of signals, such as noise and disturbances, outside of the desired frequency range; and 2) the dual-RC provides higher gain than conventional RC at the odd-harmonics. Therefore, dual-RC will improve the tracking performance of trajectories with odd-harmonics. It is noted that simply cascading two basic repetitive controllers together results in excessive gain at the even harmonics, which can degrade the system's performance for tracking odd-harmonic reference trajectories [61] and should be avoided. Readers are referred to [59] for details of the stability analysis of the dual-RC system.

Dealing with Hysteresis in RC Design

The aforementioned RC system assumes the system is linear and in particular does not have any hysteresis behavior. For details on hysteresis, see "Hysteresis and Dynamic Effects in Piezo-Based Positioning Systems." When the RC is applied to a system with hysteresis, there is no guarantee that the closed-loop RC system is stable. In fact, if not accounted for, hysteresis can drastically affect the stability of a closed-loop system.

To better illustrate the impact that hysteresis can have, consider the simulation and experimental tracking results shown in Figure 6. In Figure 6(a), simulation results show effective tracking of the desired trajectory as the operating cycle increases for a repetitive controller designed for a linear model $G(z)$ of the plant. However, the experimental results in Figure 6(b) show different behavior when the RC based on linear dynamics $G(z)$ is applied to the actual system. In particular, the response shows high frequency oscillations, indicating the onset of instability.

To handle the hysteresis behavior, several control schemes have been used. An internal feedback loop can be used to linearize the plant dynamics [62], as shown in Figure 7(a), or the hysteresis can be compensated for using model-based feedforward control, as shown in Figure 7(b) [63], [64], effectively linearizing the plant dynamics. Either of these schemes allows a repetitive controller designed based on linear dynamics to be applied to the system.

The feedforward approach assumes the plant has the cascade model structure shown in Figure 8. The hysteresis behavior is described by a rate-independent input nonlinearity $\mathcal{H}[\cdot]$ and the output of this nonlinearity drives a linear dynamics model $G(s)$, which describes the structural dynamics and creep behavior. Simple polynomial-based [65], Maxwell slip (a lumped parameter model) [66], Duhem [67], and Preisach [68], [69] models have been used to model hysteresis. Recently, the Prandtl-Ishlinskii (P-I) model [70], [71] was used to linearize the plant dynamics for RC design [59]. The P-I model consists of a smaller parameter space than, for example, the Preisach model, which permits straightforward online implementation; see "Prandtl-Ishlinskii Model for Hysteresis" for details.

RC for nonlinear systems has been studied [72]–[75], and recently the effect of hysteresis on the stability of an RC closed-loop system was analyzed [76]. Using the P-I model, the effect of hysteresis on the stability of the closed-loop RC system was analyzed to determine the tolerable *size* of the hysteresis nonlinearity. It was determined that, if the hysteresis behavior in the system was unacceptably large, a feedforward controller based on the structure of the P-I model can be used to compensate for the hysteresis behavior.

APPLICATION IN AFM NANOFABRICATION

As an illustrative application of RC, a pattern of nanosized features were created using a commercial atomic force microscope and the custom-designed nanopositioning system (scanner). Such a pattern of nanofabricated holes can

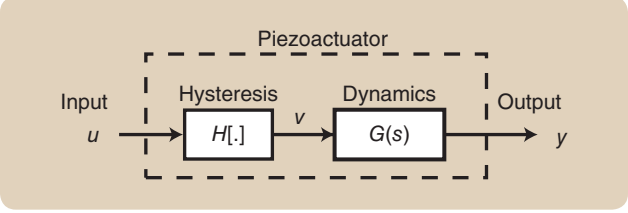

FIGURE 8 A nonlinear model for piezoactuators. The hysteresis behavior is captured by a rate-independent input nonlinearity, and the output of this nonlinearity drives a linear dynamics model that describes the dynamic effects (vibration and creep).

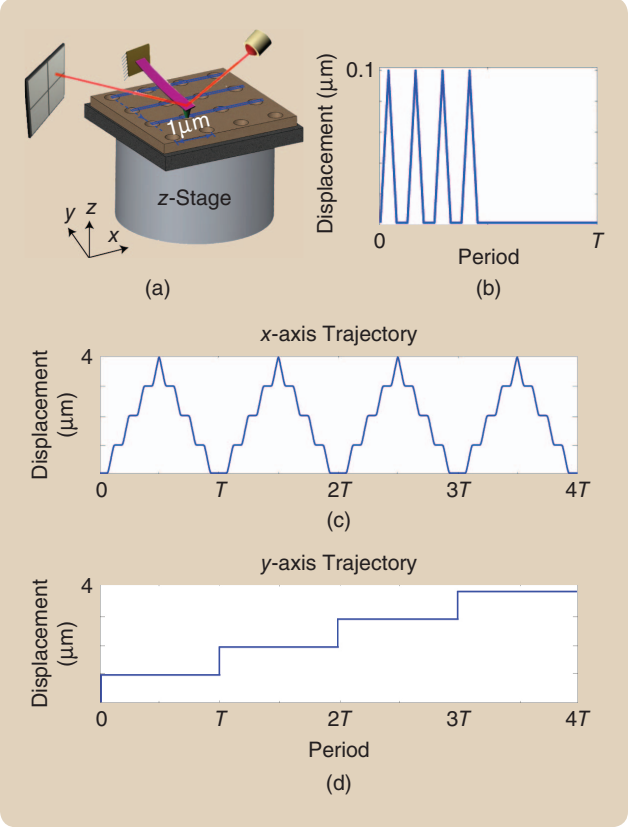

FIGURE 9 Atomic force microscopy (AFM)-based nanofabrication: (a) AFM system with microcantilever for patterning nanosized holes, (b) z-axis motion, (c) x-axis (periodic trajectory) motion, and (d) y-axis motion.

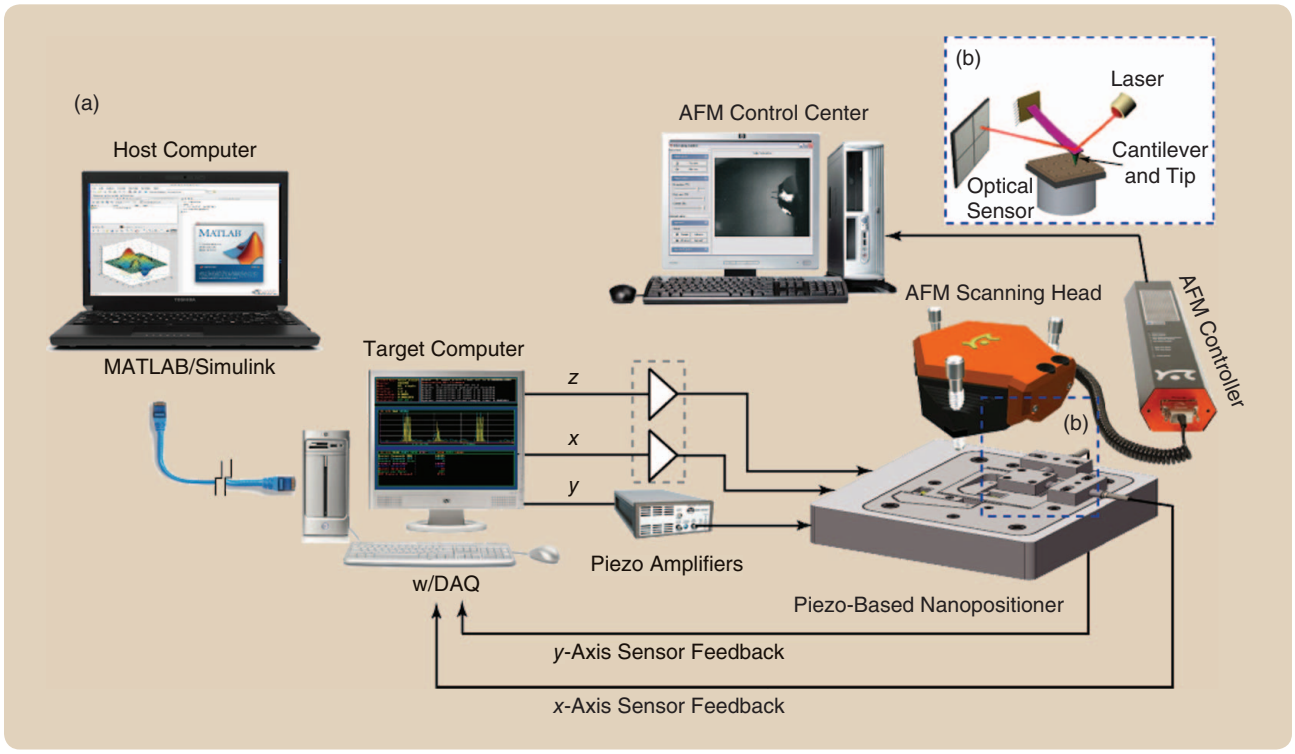

FIGURE 10 (a) Experimental nanofabrication system. (b) A close-up view of the interaction section of the nanofabrication system: AFM cantilever, tip, and the substrate for fabrication.

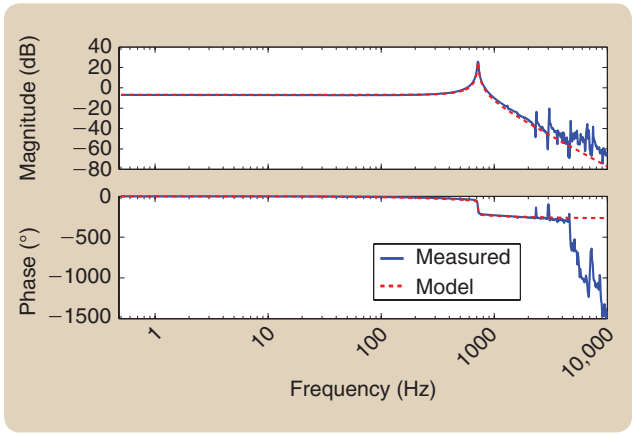

FIGURE 11 The measured frequency response (solid blue line) of the nanopositioner along the *x*-axis compared to the linear dynamic model (dashed red line).

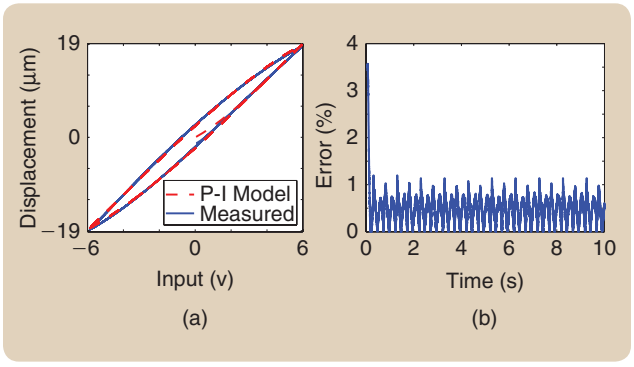

FIGURE 12 The Prandtl-Ishlinskii (P-I) hysteresis model versus the measured hysteresis. (a) The hysteresis curve. (b) The matching error between the model and the measured hysteresis.

be used for controlled growth of ZnO nanowire arrays. Below, the performance of RC is compared to traditional PID control currently employed in SPM systems.

Nanofabrication involves making structures with dimensions at nanometer level (100 nm or fewer). Techniques to create nanosize features include photolithography, nanoimprint, self-assembly, and SPM (such as STM and AFM). Recently, AFM has attracted great attention as a viable option for fabricating a wide range of nanostructures. AFM-based nanofabrication technologies mainly include nanomanipulation, force lithography, nanografting, nanooxidation, and dip-pen nanolithography [77]. The benefits of using AFM include: 1) the ability to simultaneously fabricate and visualize nanostructures with the same equipment, 2) fabrication can be performed in a standard room environment, 3) fabrication can be done on different materials (for example, metals, semiconductors, polymers, organic substrates), and 4) the cost is lower compared to batch fabrication techniques. The force-lithography approach is chosen for creating patterns of nanosized holes on a polymethylmethacrylate (PMMA) layer that has been spin coated on a ZnO substrate. The force-lithography approach simply uses the atomic force microscope tip

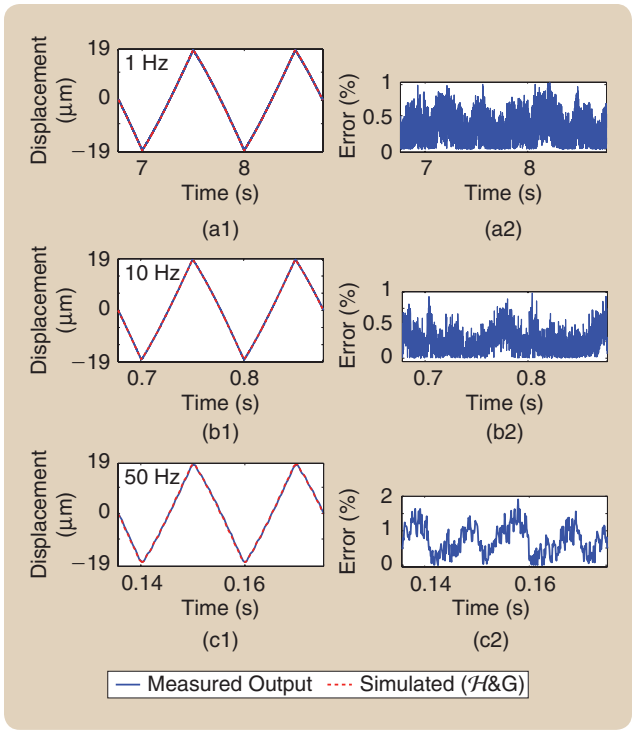

FIGURE 13 Experimental results to validate the cascade model structure shown in Figure 8: (a1) and (a2) displacement and error versus time comparing the measured response (solid line) and model output (dashed line) for scanning at 1 Hz, (b1) and (b2) for scanning at 10 Hz, and (c1) and (c2) for scanning at 50 Hz.

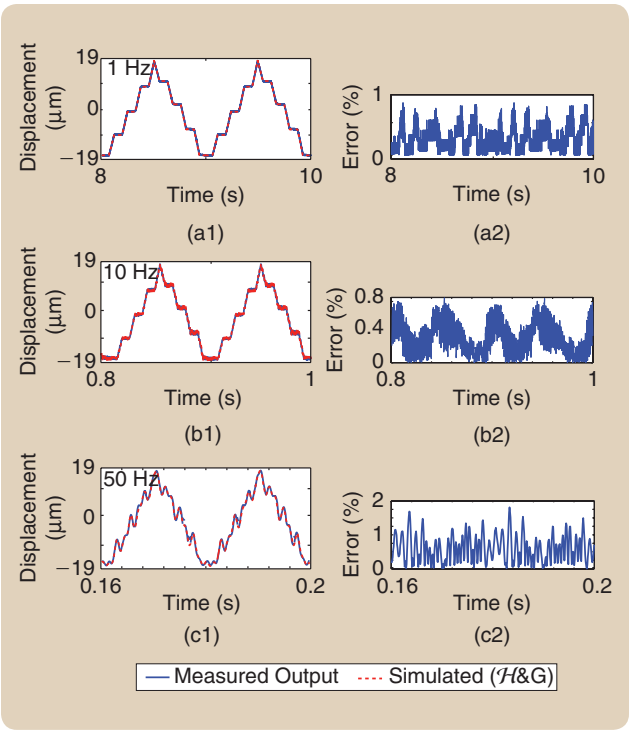

FIGURE 14 Experimental results to validate the cascade model structure shown in Figure 8 using inputs for nanofabrication: (a1) and (a2) displacement and error versus time comparing the measured response (solid line) and model output (dashed line) for scanning at 1 Hz, (b1) and (b2) for scanning at 10 Hz, and (c1) and (c2) for scanning at 50 Hz.

to mechanically deform the PMMA layer to create a nanosized hole. These holes can then be used for controlled growth of zinc oxide nanostructures, such as nanoscale ZnO nanowires.

The Experimental Nanofabrication System

The AFM-based nanofabrication process is illustrated in Figure 9, where the desired motions along the x (c), y (d), and z (b) directions are shown. During the fabrication process, the probe was held fixed laterally and actuated in the z-direction to produce an indentation on the surface [see Figure 9(c) and (d)]. The raster scan pattern illustrated in Figure 9(c) is a periodic trajectory. In the experiments, RC was used to control the motion along the x-axis, and a PID controller was used to control the y-axis. The experimental nanofabrication system is shown in Figure 10, which consists of custom-designed piezo-based, three-axis serial-kinematic nanopositioner (range $40 \times 40 \times 2.5$ μm, with x/y resonances of 718.5 Hz/532.2 Hz, respectively, both in the actuation direction) and a commercial AFM scanhead (Nanosurf easyScan 2). The stage was outfitted with inductive sensors (Kaman SMU9000-15N) to measure displacement in the lateral (x and y) directions. The controllers were implemented using the Matlab xPC Target system with a maximum closed-loop sampling frequency of 10 kHz.

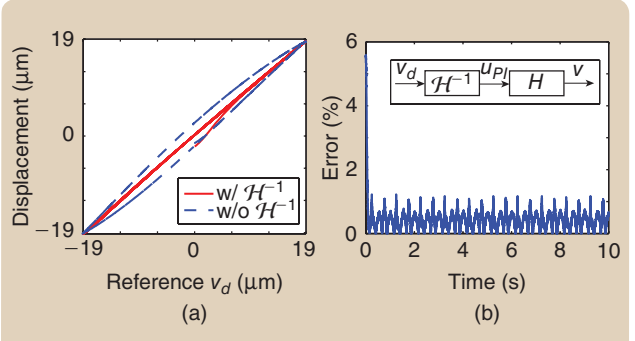

FIGURE 15 Performance of the inverse hysteresis compensator: (a) The hysteresis curves for the piezoactuator with (solid line) and without (dashed line) feedforward compensation. (b) The tracking error.

The sample was prepared for nanofabrication, and the basic steps are: a) coat a ZnO buffer layer onto a Si substrate; b) spin coat the resist layer, such as polymethylmethacrylate (PMMA), onto the ZnO layer for patterning; and c) pattern the resist layer using the atomic force microscope (scratching) operating under RC. The focus of the experiment was to create the pattern of nanosized holes on the PMMA layer and evaluate the effectiveness of the RC approach, and so the final growth of the ZnO nanowires through chemical reaction in solution is not discussed.

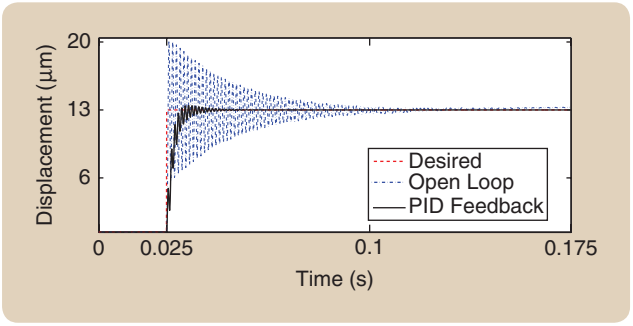

FIGURE 16 Comparison of open-loop step response and setpoint tracking obtained by proportional-integral-differential control.

System Modeling

The x-axis of the nanopositioner was modeled for controller design and implementation. First, the linear dynamics model was obtained by curve fitting the measured frequency response between 0.5 Hz to 3 kHz. The measured frequency response is shown by the solid line and the model is represented by the dashed line in Figure 11. The transfer function model is

$$G(s) = \frac{3.391 \times 10^{10}}{s^3 + 3759s^2 + 2.063 \times 10^7 s + 7.514 \times 10^{10}}. \quad (8)$$

The discrete-time model was obtained using the Matlab command 'c2d' with a sampling frequency of 10 kHz, and the model is

$$G(z) = \frac{0.001304z^3 + 0.01319z^2 + 0.01224z + 0.001041}{z^3 - 2.485z^2 + 2.233z - 0.6867}. \quad (9)$$

The hysteresis behavior in the x-axis was modeled using the P-I approach. The parameters for the P-I model are $g_0 = 0.658$, $g_1 = 0.0606$, $\lambda = 0.6684$, $\delta = 0.6859$, and $\rho = 0.3569$ [59]. The output of the P-I model is compared to the measured response in Figure 12. The modeling error is shown in Figure 12(b), where the maximum error at steady state is approximately 1.15%.

Both the hysteresis and dynamics models were combined to validate the cascade model structure shown in Figure 8. The results are shown in Figures 13–14. The maximum modeling error is less than 1.9% for scanning up to 50 Hz (see plot (a1)–(c2) in Figure 13). The maximum modeling error for the nanofabrication signal is less than 1.7% up to 50 Hz scanning (see plot (a1)–(c2) in Figure 14). Therefore, the dynamics and hysteresis models are judged to be accurate predictors of the behavior of the nanopositioner.

Inverse Hysteresis Compensator

An inverse hysteresis compensator was designed for the high-speed x-axis of the nanopositioner to account for the hysteresis behavior for RC design. The parameters of the inverse hysteresis compensator are $g_0' = 1.4188$, $g_1' = -0.1582$, $\lambda' = 0.2873$, $\delta' = 0.5769$, and $\rho' = 0.7521$ [59]. The results of the inverse hysteresis compensator are shown in Figure 15; specifically, plot (a) compares the response of the system with and without the feedforward hysteresis compensator. As shown in plot (b), the tracking error at steady-state is less than 1.3%, demonstrating the effectiveness of the compensator to minimize the hysteresis behavior.

Controller Design and Implementation

To design the repetitive controller, the first task was to design the feedback controller $G_c(z)$ as shown in Figure 3. In this case, $G_c(z)$ was chosen as a PID controller, with transfer function

$$G_c(z) = k_p + k_i \frac{T_s z}{z-1} + k_d \frac{z-1}{T_s z}, \quad (11)$$

where $T_s = 10$ kHz is the sampling frequency. The controller parameters are $k_p = 0.02$, $k_i = 1000$, and $k_d = 0.0001$. The step response of the system under PID control is shown in Figure 16. The open-loop response without control has significant overshoot, a long settling time, and noticeable creep. With PID control, the overshoot and creep were minimized.

Next, the low-pass filter was chosen as

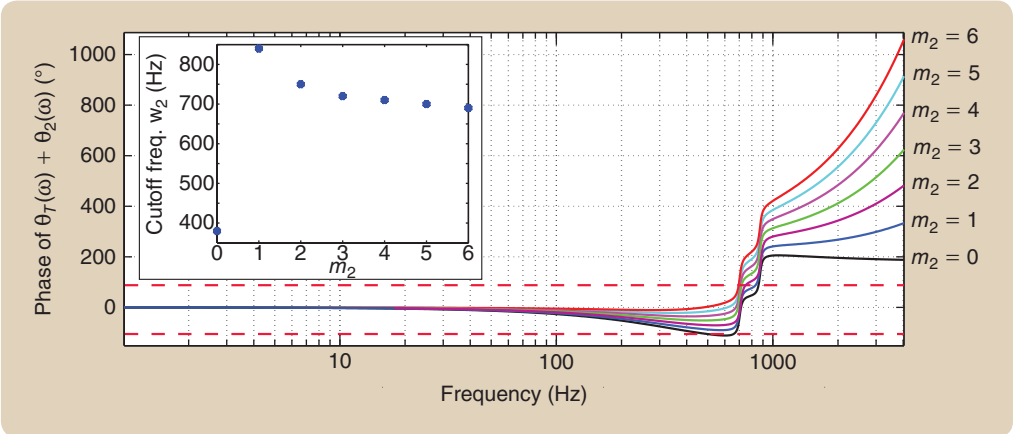

FIGURE 17 Phase response of $\theta_T(\omega) + \theta_2(\omega)$, where $\theta_2(\omega)$ is the phase of the lead compensator $P_2(z) = z^{m_2}$. The inset plot shows the cutoff frequency as a function of the phase lead parameter m_2. The objective is to operate within the frequency range established by the ±90° crossover, hence $m_2 = 1$ offers the largest frequency range.

$$Q(z) = \frac{a}{z+b}, \qquad \text{with } a = 0.2696 \text{ and } b = -0.7304,$$

where the cutoff frequency is 500 Hz (sampling frequency of $T_s = 10$ kHz). The cutoff frequency was determined by the phase response of $\theta_T(\omega) + \theta_2(\omega)$ for different values of the phase lead parameter m_2, as shown in Figure 17. The inset in Figure 17 shows the ±90° crossover frequency as a function of the phase lead parameter m_2. From the phase response, when $m_2 = 0$, the ±90° crossover frequency for $\theta_T(\omega) + \theta_2(\omega)$ is approximately 380 Hz. When $m_2 = 1$, the value is approximately 800 Hz. Thus, the cutoff frequency for $Q(z)$ was chosen as 500 Hz and phase lead of $m_2 = 1$ was used. For higher rate fabrication, the cutoff frequency can be increased, but only up to 800 Hz when $m_2 = 1$ (see Figure 17).

Using the linear dynamics model, simulation was used to determine the optimum values for the RC gain k_{rc} and the phase lead parameter, m_1. For details, see [36] and [59]. The values for the experiment were chosen as $k_{\text{rc}} = 0.4$ and $m_1 = 4$.

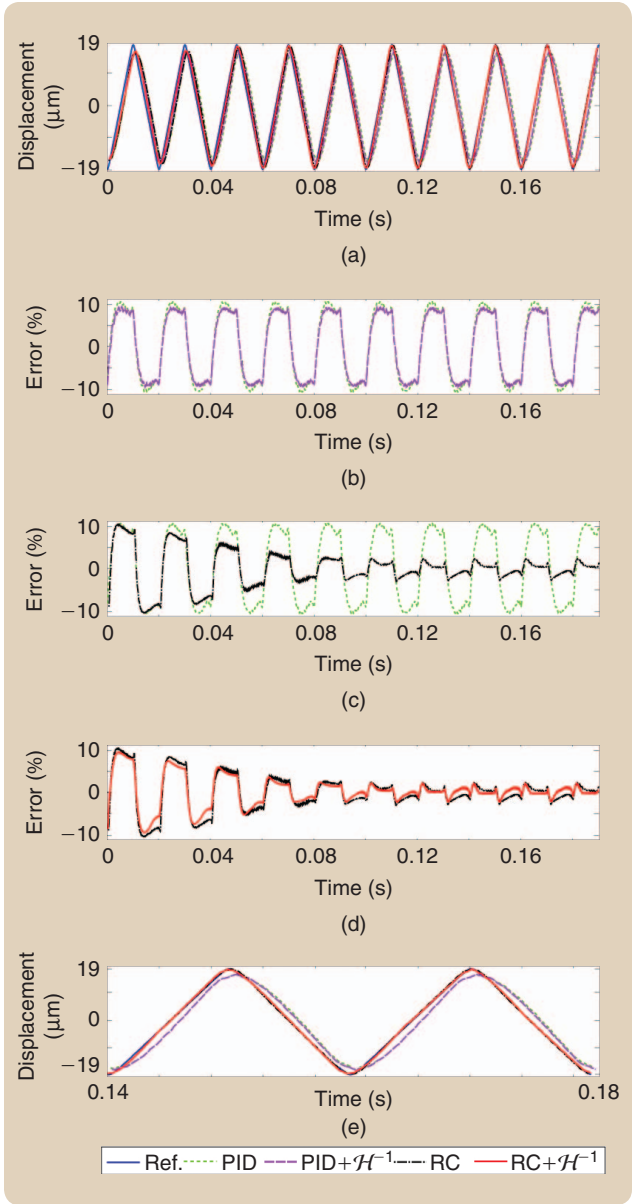

FIGURE 18 (a) Experimentally measured tracking results of a triangular trajectory at 50 Hz for proportional-integral-derivative (PID), PID with $\mathcal{H}^{-1}$, repetitive control (RC), and RC with $\mathcal{H}^{-1}$. Experimentally measured tracking error at 50 Hz comparing (b) PID with and without $\mathcal{H}^{-1}$, (c) PID and RC (without $\mathcal{H}^{-1}$), (d) PID+RC and PID+RC+$\mathcal{H}^{-1}$, and (e) steady-state displacement versus time.

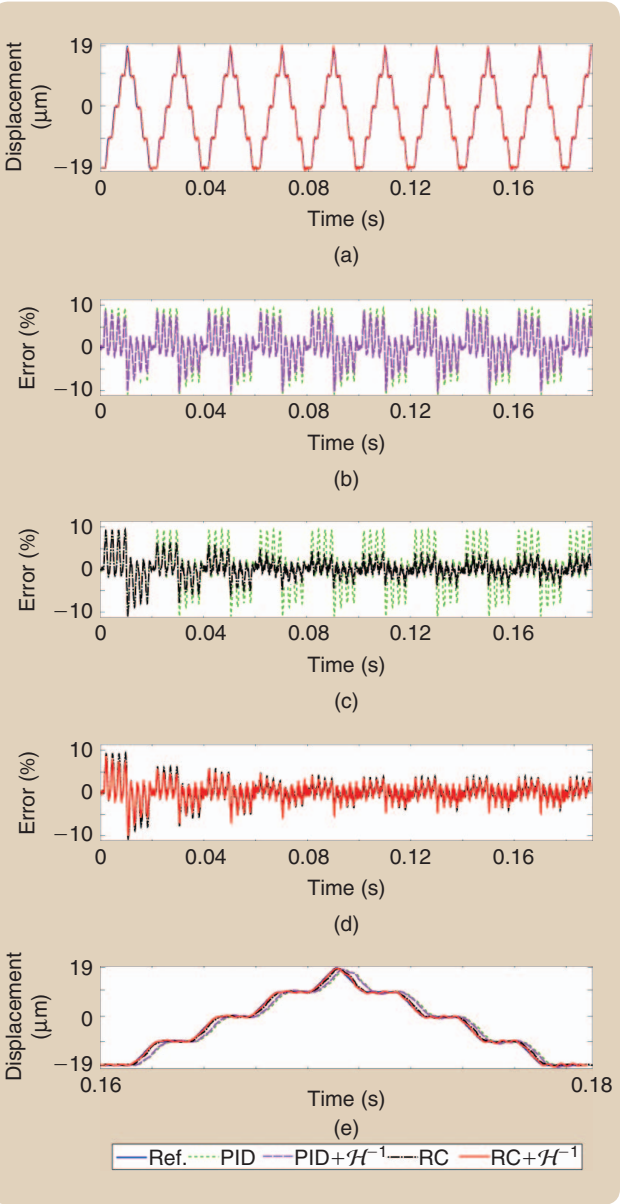

FIGURE 19 (a) Experimentally measured tracking results of nanofabrication trajectory at 50 Hz for proportional-integral-derivative (PID), PID with $\mathcal{H}^{-1}$, repetitive control (RC), and RC with $\mathcal{H}^{-1}$. Experimentally measured tracking error at 50 Hz comparing (b) PID with and without $\mathcal{H}^{-1}$, (c) PID and RC (without $\mathcal{H}^{-1}$), (d) PID+RC and PID+RC+$\mathcal{H}^{-1}$, and (e) steady-state displacement versus time.

TABLE 3 Steady-state tracking error for a triangle reference signal.

Controller	1 Hz		10 Hz		50 Hz	
	e_{max} (%)	e_{rms} (%)	e_{max} (%)	e_{rms} (%)	e_{max} (%)	e_{rms} (%)
PID	1.8	1.49	4.3	3.12	10.6	7.59
PID + $\mathcal{H}^{-1}$	1.5	1.19	3.6	2.36	9.3	6.80
PID + RC	0.5	0.21	1.3	0.51	2.5	0.89
PID + RC + $\mathcal{H}^{-1}$	0.4	0.16	1.2	0.44	2.2	0.78

TABLE 4 Steady-state tracking error for a nanofabrication reference signal.

Controller	1 Hz		10 Hz		50 Hz	
	e_{max} (%)	e_{rms} (%)	e_{max} (%)	e_{rms} (%)	e_{max} (%)	e_{rms} (%)
PID	3.90	3.16	5.81	4.38	10.8	8.48
PID + $\mathcal{H}^{-1}$	3.62	2.64	4.96	3.68	10.1	7.80
PID + RC	0.91	0.40	1.93	0.75	3.90	1.52
PID + RC + $\mathcal{H}^{-1}$	0.87	0.34	1.85	0.69	3.74	1.46

Tracking and Fabrication Results

Here experimental tracking results are presented to compare the response of PID, PID with $\mathcal{H}^{-1}$, RC, and RC with $\mathcal{H}^{-1}$ control systems for scanning up to 50 Hz. Tracking results for two different reference trajectories are shown in Figures 18 and 19. The steady-state tracking errors for both cases are presented in Tables 3 and 4, respectively. Specifically, the maximum error [e_{max}(%)] and root-mean-squared error [e_{rms}(%)] are reported. Because the action of the repetitive controller was delayed by one scan period, the tracking response for the first period was similar for the PID and RC, as shown in Figures 18 and 19. However, after the first period the RC begins to take action, as illustrated by the reduction in the tracking error from one cycle to the next. In contrast, the tracking error of the PID controller persists from one cycle to the next.

The tracking results demonstrate that the RC controller reduces the maximum steady-state tracking error from 10.6 to 2.5%, compared to PID for tracking a triangular trajectory, and reduces the maximum tracking error from 10.8 to 3.9% for tracking the nanofabrication trajectory. The reductions are 76.4 and 63.9%, respectively. Including $\mathcal{H}^{-1}$ with the PID and RC controllers results in an additional reduction in the tracking error. For example, by adding the $\mathcal{H}^{-1}$ to RC controller, the tracking error of PID controller decreases from 10.6 to 2.2%, a total 79.3% reduction, for triangular trajectory tracking. For the nanofabrication trajectory tracking, the total decrease is 65.4%, and the maximum tracking error was only 3.74%. RC with $\mathcal{H}^{-1}$ provided the best performance compared to traditional PID control.

Next, the control systems are compared for fabricating nanosize features with a pitch of 1 µm. The features were fabricated on the PMMA-coated ZnO/Si substrate. The deposited PMMA layer was approximately 25-nm thick, coated in-house on a 40-nm layer of ZnO that was deposited on a Si substrate. Figure 20 shows how the layers are arranged and attached to the sample stage of the nanopositioner. All of the features were fabricated and imaged using the nanofabrication system shown in Figure 10, and the experiments were performed in air at room temperature. During fabrication and imaging, the AFM scan head was operated in contact constant-force mode. The atomic force microscope tips used were Vistaprobes silicon tips (T190R-10, nanoScience) with a tip radius of approximately 10 nm and a spring constant of approximately 48 N/m. During fabrication, the AFM scanner positions the cantilever tip above the sample surface with a desired force (load), and the nanopositioner was controlled to displace the

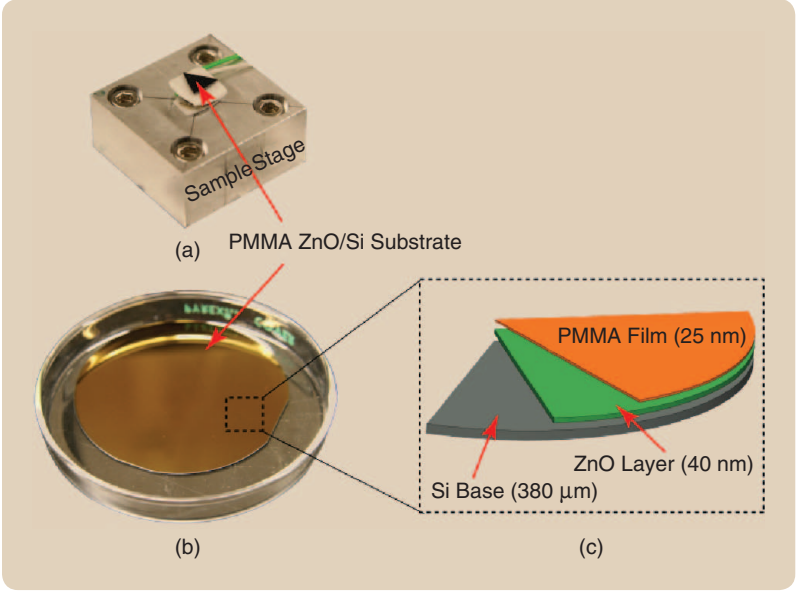

FIGURE 20 Photograph of the ZnO/Si substrate coated with PMMA film: (a) the PMMA-coated ZnO/Si substrate on the sample stage of the nanopositioner, (b) the PMMA-coated ZnO/Si wafer, and (c) a schematic diagram of the layers of the sample.

This article focuses on the design and control of nanopositioning systems (nanopositioners) that operate mostly in a repetitive fashion.

sample laterally (in the x and y directions) and vertically to create the nanosized holes on the surface.

For fabrication experiments, the signals shown in Figure 9(b)–(d) were applied to the z, x, and y axis of the nanopositioner. The AFM images of the PMMA film surface after patterning are shown in Figure 21. These images were scanned using the NanoSurf atomic force microscope scanhead with the nanopositioner. The images in Figure 21 show features fabricated in open loop, with PID and $\mathcal{H}^{-1}$, and with RC and $\mathcal{H}^{-1}$ at scanning rates of 1, 10, and 50 Hz. From the images, it can be observed that the RC with $\mathcal{H}^{-1}$ controller enabled fabrication of features with less distortion compared to the other two cases. Particularly at high scan rates, the open-loop and PID controller responses, which previously showed significant tracking error, also lead to distortion in the fabrication process, such as holes that were not evenly spaced and variations in the dimensions of the features. The damage was caused by the vibration of the nanopositioner along the fast scanning (x) direction. By implementing the PID with the inverse hysteresis compensator, the quality of the fabricated nanohole arrays increases compared to the open loop case. However, the improvement in the quality is limited, for example at 50 Hz, the damage caused by the atomic force microscope tip was still significant. By adding RC to the PID and $\mathcal{H}^{-1}$ control system, the distortion was reduced. Therefore, the RC approach provides a means for improved fabrication of nanofeatures at high speed.

CONCLUDING REMARKS

Multi-axis nanopositioning stages are critical in many micro- and nanoscale applications. This article discussed the process of mechanical design that takes control into account, namely designing the positioning stage with dynamics that are "well behaved," such that simple models capture the dynamics effectively. For precision tracking of periodic motion trajectories common in nanopositioning applications, the repetitive control approach was described. This approach was applied to nanofabrication to show significant improvement in tracking performance for fabricating nanosized features on a PMMA coated ZnO/Si substrate.

ACKNOWLEDGMENTS

The authors thank Brian Kenton for help in designing and fabricating the nanopositioners used in the experiments. The authors gratefully acknowledge support from National Science Foundation (NSF) Grant CMMI 0910570, DUE 0852756, CMMI 1126582, and the Nevada NASA Space Grant Consortium. Additionally, the authors are grateful to Dr. A.J. Fleming for the insightful discussions and providing the PiezoDrive (www.piezodrive.com) amplifiers for the experimental work.

AUTHOR INFORMATION

Yingfeng Shan received the M.S. degree in mechanical engineering from Virginia Commonwealth University, Richmond, in 2008 and the Ph.D. degree from the University of Nevada, Reno in 2011. From 2005 to 2006, he was a control engineer at China National Petroleum Corporation, China. He is currently employed by ESI, Portland, Oregon, working on high-precision positioning systems.

Kam K. Leang (kam@unr.edu) received the B.S. and M.S. degrees in mechanical engineering from the University of Utah, Salt Lake City, in 1997 and 1999, respectively,

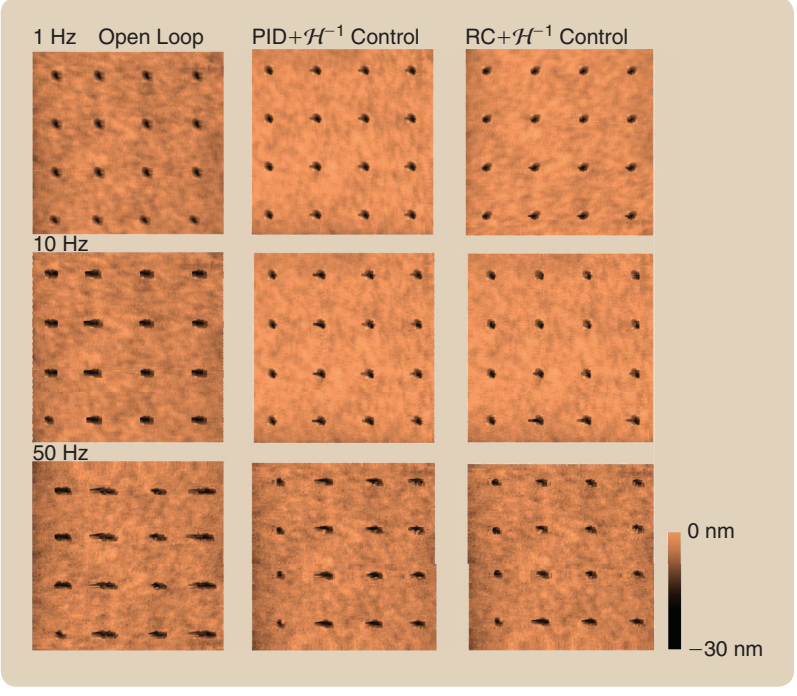

FIGURE 21 Images of nanofabrication with open-loop, proportional-integral-derivative control with hysteresis compensation, and repetitive control with hysteresis compensation.

and the Ph.D. degree from the University of Washington, Seattle, in December 2004. He is an associate professor in the Department of Mechanical Engineering at the University of Nevada-Reno, which he joined in 2008. His research interests include mechanical design, modeling, and control of piezo-driven systems for nanopositioning applications, such as scanning probe microscopy, fabrication and control of electroactive polymers, mechatronic system design, and autonomous systems. He is a member of ASME, IEEE, and SPIE. He can be contacted at 1664 N. Virginia ST MS312, Reno, Nevada, 89557-0312 USA.

REFERENCES

[1] Y. Yuen, S. O. R. Moheimani, B. J. Kenton, and K. K. Leang, "Invited Review: High-speed flexure-guided nanopositioning: Mechanical design and control issues," *Rev. Sci. Instru*., vol. 83, no. 12, article 121101, 2012.

[2] D. Kang and D. Gweon, "Development of flexure based 6-degrees of freedom parallel nano-positioning system with large displacement," *Rev. Sci. Instrum*., vol. 83, no. 3, article 035003, 2012.

[3] Y. Okazaki, "A micro-positioning tool post using a piezoelectric actuator for diamond turning machines," *Precis. Eng.*, vol. 12, no. 3, pp. 151–156, 1990.

[4] W. Gao, R. J. Hocken, J. A. Patten, J. Lovingood, and D. A. Lucca, "Construction and testing of a nanomachining instrument," *Precis. Eng.*, vol. 24, no. 4, pp. 320–328, 2000.

[5] Y. Martin and H. K. Wickramasinghe, "Toward accurate metrology with scanning force microscopes," *J. Vac. Sci. Technol. B*, vol. 13, no. 6, pp. 2335–2339, 1995.

[6] W. Gao, *Precision Nanometrology: Sensors and Measuring Systems for Nanomanufacturing.* New York: Springer-Verlag, 2010.

[7] T. Ando, T. Uchihashi, and T. Fukuma, "High-speed atomic force microscopy for nanovisualization of dynamic biomolecular processes," *Prog. Surf. Sci*., vol. 83, nos. 7–9, pp. 337–437, 2008.

[8] D. Croft, G. Shed, and S. Devasia, "Creep, hysteresis, and vibration compensation for piezoactuators: Atomic force microscopy application," *ASME J. Dyn. Syst. Meas. Control*, vol. 123, no. 1, pp. 35–43, 2001.

[9] S. Devasia, E. Eleftheriou, and S. O. R. Moheimani," A survey of control issues in nanopositioning," *IEEE Trans. Control Syst. Technol*., vol. 15, no. 5, pp. 802–823, 2007.

[10] J. H. Kindt, G. E. Fantner, J. A. Cutroni, and P. K. Hansma, "Rigid design of fast scanning probe microscopes using finite element analysis," *Ultramicroscopy*, vol. 100, nos. 3–4, pp. 259–265, 2004.

[11] Y. K. Yong, S. S. Aphale, and S. O. R. Moheimani, "Design, identification, and control of a flexure-based xy stage for fast nanoscale positioning," *IEEE Trans. Nanotechnol*., vol. 8, no. 1, pp. 46–54, 2009.

[12] B. J. Kenton, and K. K. Leang, "Design and control of a three-axis serial-kinematic high-bandwidth nanopositioner," *IEEE/ASME Trans. Mechatron*., vol. 17, no. 2, pp. 356–369, 2012.

[13] G. Schitter, K. J. Astrom, B. E. DeMartini, P. J. Thurner, K. L. Turner, and P. K. Hansma, "Design and modeling of a high-speed AFM-scanner," *IEEE Trans. Control Syst. Technol*., vol. 15, no. 5, pp. 906–915, 2007.

[14] K. K. Leang, Q. Zou, and S. Devasia, "Feedforward control of piezoactuators in atomic force microscope systems: Inversion-based compensation for dynamics and hysteresis," *IEEE Control Syst. Mag.*, vol. 29, no. 1, pp. 70–82, 2009.

[15] G. M. Clayton, S. Tien, K. K. Leang, Q. Zou, and S. Devasia, "A review of feedforward control approaches in nanopositioning for high speed SPM," *ASME J. Dyn. Syst. Meas. Control*, vol. 131, no. 6, pp. 061101–061119, 2009.

[16] E. Eleftheriou and S. O. R. Moheimani, *Control Technologies for Emerging Micro and Nanoscale Systems.* New York: Springer-Verlag, 2011.

[17] R. C. Barrett and C. F. Quate, "Optical scan-correction system applied to atomic force microscopy," *Rev. Sci. Instrum*., vol. 62, no. 6, pp. 1393–1399, 1991.

[18] R. J. E. Merry, N. C. T. de Kleijn, M. J. G. van de Molengraft, and M. Steinbuch, "Using a walking piezo actuator to drive and control a high precision stage," *IEEE/ASME Trans. Mechatron*., vol. 14, no. 1, pp. 21–31, 2009.

[19] S. Korson and A. J. Helmicki, "An H_∞ based controller for a gas turbine clearance control system," in *Proc. 4th IEEE Conf. Control Applications*, Albany, NY, Sept. 1995, pp. 1154–1159.

[20] S. Salapaka, A. Sebastin, J. P. Cleveland, and M. V. Salapaka, "High bandwidth nano-positioner: A robust control approach," *Rev. Sci. Instrum*., vol. 73, no. 9, pp. 3232–3241, 2002.

[21] B. Bhikkaji, M. Ratnam, A. J. Fleming, and S. O. R. Moheimani, "High-performance control of piezoelectric tube scanners," *IEEE Trans. Control Syst. Technol*., vol. 15, no. 5, pp. 853–866, 2007.

[22] B. Bhikkaji, M. Ratnam, and S. O. R. Moheimani, "PVPF control of piezoelectric tube scanners," *Sens. Actuators A, Phys*., vol. 135, no. 2, pp. 700–712, 2007.

[23] S. S. Aphale, A. J. Fleming, and S. O. R. Moheimani, "High speed nanoscale positioning using a piezoelectric tube actuator with active shunt control," *Micro Nano Lett*., vol. 2, no. 1, pp. 9–12, 2007.

[24] A. J. Fleming and A. G. Wills, "Optimal periodic trajectories for band-limited systems," *IEEE Control Syst. Technol*., vol. 17, no. 3, pp. 552–562, 2009.

[25] K. K. Leang and S. Devasia, "Design of hysteresis-compensating iterative learning control for piezo positioners: Application to atomic force microscopes," *Mechatronics*, vol. 16, nos. 3–4, pp. 141–158, 2006.

[26] Y. Wu and Q. Zou, "Iterative control approach to compensate for both the hysteresis and the dynamics effects of piezo actuators," *IEEE Control Syst. Technol*., vol. 15, no. 5, pp. 936–944, 2007.

[27] M. Radmacher, "Measuring the elastic properties of biological samples with the AFM," *IEEE Eng. Med. Biol*., vol. 16, no. 2, pp. 47–57, 1997.

[28] S. M. Salapaka and M. V. Salapaka, "Scanning probe microscopy," *IEEE Control Syst. Mag*., vol. 28, no. 2, pp. 65–83, 2008.

[29] S.-H. Lee and T. J. Royston, "Modeling piezoceramic transducer hysteresis in the structural vibration control problem," *J. Acoust. Soc. Amer*., vol. 108, no. 6, pp. 2843–2855, 2000.

[30] R. Oboe, A. Beghi, and B. Murari, "Modeling and control of a dual stage actuator hard disk drive with piezoelectric secondary actuator," in *Proc. IEEE/ASME Advanced Intelligent Mechatronics*, 1999, pp. 138–143.

[31] G. Schitter, "Improving the speed of AFM by mechatronic design and modern control methods," *Techn. Messen*, vol. 76, no. 5, pp. 266–273, 2009.

[32] A. J. Fleming, "Dual-stage vertical feedback for high speed-scanning probe microscopy," *IEEE Trans. Control Syst. Technol*., vol. 19, no. 1, pp. 156–165, 2011.

[33] B. A. Francis and W. M. Wonham, "The internal model principle of control theory," *Automatica*, vol. 12, no. 5, pp. 457–465, 1976.

[34] T. Inoue, M. Nakano, and S. Iwai, "High accuracy control of a proton synchrotron magnet power supply," in *Proc. 8th IFAC World Congr*., 1981, vol. 20, pp. 216–221.

[35] S. Hara, Y. Yamamoto, T. Omata, and M. Nakano, "Repetitive control system: A new type servo system for periodic exogenous signals," *IEEE Trans. Autom. Contr*., vol. 33, no. 7, pp. 659–668, 1988.

[36] U. Aridogan, Y. Shan, and K. K. Leang, "Design and analysis of discrete-time repetitive control for scanning probe microscopes," *ASME J. Dyn. Syst. Meas. Control*, vol. 131, no. 6, article 061103, 2009.

[37] K. K. Chew and M. Tomizuka, "Digital control of repetitive errors in disk drive systems," *IEEE Control Syst. Mag*., vol. 10, no. 1, pp. 16–20, 1990.

[38] M. Steinbuch, S. Weiland, and T. Singh, "Design of noise and period-time robust high-order repetitive control, with application to optical storage," *Automatica*, vol. 43, no. 12, pp. 2086–2095, 2007.

[39] C. J. Li and S. Y. Li, "To improve work-piece roundness in precision diamond turning by in situ measurement and repetitive control," *Mechatronics*, vol. 6, no. 5, pp. 523–535, 1996.

[40] S.-L. Chen and T.-H. Hsieh, "Repetitive control design and implementation for linear motor machine tool," *Int. J. Mach. Tools Manuf*., vol. 47, nos. 12–13, pp. 1807–1816, 2007.

[41] S. Arimoto, S. Kawamura, and F. Miyazaki, "Bettering operation of robots by learning," *J. Robot. Syst*., vol. 1, no. 2, pp. 123–140, 1984.

[42] K. L. Moore, M. Dahleh, and S. P. Bhattacharyya, "Iterative learning control: A survey and new results," *J. Robot. Syst*., vol. 9, no. 5, pp. 563–594, 1992.

[43] D. A. Bristow, M. Tharayil, and A. G. Alleyne, "A survey of iterative learning control," *IEEE Control Syst. Mag*., vol. 26, no. 3, pp. 96–114, 2006.

[44] F. Lowrie, M. Cain, M. Stewart, and M. Gee, "Time dependent behaviour of piezo-electric materials," Natl Phys. Lab., New Delhi, India, Tech. Rep. 151, 1999.

[45] H.-J. Lee and D. A. Saravanos, "The effect of temperature dependent material properties on the response of piezoelectric composite materials," *J. Intell. Mater. Syst. Struct*., vol. 9, no. 7, pp. 503–508, 1998.

[46] G. E. Fantner, P. Hegarty, J. H. Kindt, G. Schitter, G. A. G. Cidade, and P. K. Hansma, "Data acquisition system for high speed atomic force microscopy," *Rev. Sci. Instrum*., vol. 76, no. 2, article 026118, 2005.

[47] B. J. Kenton, A. J. Fleming, and K. K. Leang, "A compact ultra-fast vertical nanopositioner for improving SPM scan speed," *Rev. Sci. Instrum.*, vol. 82, no. 12, article 123703, 2011.
[48] S.-C. Chen and M. L. Culpepper, "Design of a six-axis micro-scale nanopositioner—μhexflex," *Precis. Eng.*, vol. 30, no. 3, pp. 314–324, 2006.
[49] N. B. Hubbard, M. L. Culpepper, and L. L. Howell, "Actuators for micropositioners and nanopositioners," *Appl. Mech. Rev.*, vol. 59, no. 6, pp. 324–334, 2006.
[50] F. E. Scire and E. C. Teague, "Piezodriven 50-μm range stage with subnanometer resolution," *Rev. Sci. Instrum.*, vol. 49, no. 12, pp. 1735–1740, 1978.
[51] G. Schitter, P. J. Thurner, and P. K. Hansma, "Design and input-shaping control of a novel scanner for high-speed atomic force microscopy," *Mechatronics*, vol. 18, nos. 5–6, pp. 282–288, 2008.
[52] K. K. Leang and A. J. Fleming, "High-speed serial-kinematic AFM scanner: Design and drive considerations," *Asian J. Control,* vol. 11, no. 2, pp. 144–153, 2009.
[53] B. J. Kenton and K. K. Leang, "Design, characterization, and control of a monolithic three-axis high-bandwidth nanopositioning stage," in *Proc. American Control Conf.,* Baltimore, MD, June 30–July 2, 2010, pp. 4949–4956.
[54] K. K. Leang and S. Devasia, "Feedback-linearized inverse feedforward for creep, hysteresis, and vibration compensation in AFM piezoactuators," *IEEE Trans. Control Syst. Technol.*, vol. 15, no. 5, pp. 927–935, 2007.
[55] J. A. Main and E. Garcia, "Piezoelectric stack actuators and control system design: Strategies and pitfalls," *AIAA J. Guid. Control, Dyn.*, vol. 20, no. 3, pp. 479–485, 1997.
[56] J. Leyva-Ramos, G. Escobar, P. R. Martinez, and P. Mattavelli, "Analog circuits to implement repetitive controllers for tracking and disturbance rejection of periodic signals," *IEEE Trans. Circuits Syst.*, vol. 52, no. 8, pp. 466–470, 2005.
[57] G. Escobar, P. R. Martinez, and J. Leyva-Ramos, "Analog circuits to implement repetitive controllers with feedforward for harmonic compensation," *IEEE Trans. Ind. Electron.*, vol. 54, no. 1, pp. 567–573, 2007.
[58] I. A. Mahmood and S. O. R. Moheimani, "Making a commercial AFM more accurate and faster using positive position feedback control," *Rev. Sci. Instrum.*, vol. 80, no. 6, article 063705, 2009.
[59] Y. Shan and K. K. Leang, "Dual-stage repetitive control with Prandtl-Ishlinskii hysteresis inversion for piezo-based nanopositioning," *Mechatronics*, vol. 22, no. 3, pp. 271–281, 2012.
[60] B.-S. Kim and T.-C. Tsao, "A performance enhancement scheme for robust repetitive control system," *ASME J. Dyn. Syst. Meas. Control*, vol. 126, no. 1, pp. 224–229, 2004.
[61] R. Costa-Castello, R. Grino, and E. Fossas, "Odd-harmonic digital repetitive control of a single-phase current active filter," *IEEE Trans. Power Electron.*, vol. 19, no. 4, pp. 1060–1068, 2004.
[62] G. S. Choi, Y. A. Lim, and G. H. Choi, "Tracking position control of piezoelectric actuators for periodic reference inputs," *Mechatronics*, vol. 12, no. 5, pp. 669–684, 2002.
[63] H.-S. Ahn, "Design of a repetitive control system for a piezoelectric actuator based on the inverse hysteresis model," in *4th Int. Conf. Control Automation*, Montreal, QC, Canada, June 10–12, 2003, pp. 128–132.
[64] Y. Shan and K. K. Leang, "Repetitive control with Prandtl-Ishlinskii hysteresis inverse for piezo-based nanopositioning," in *Proc. American Control Conf.,* St. Louis, MO, June 10–12, 2009, pp. 301–306.
[65] M. Hu, H. Du, S.-F. Ling, Z. Zhou, and Y. Li, "Motion control of an electrostrictive actuator," *Mechatronics*, vol. 14, no. 2, pp. 153–161, 2004.
[66] M. Goldfarb and N. Celanovic, "Modeling piezoelectric stack actuators for control of micromanipulation," *IEEE Control Syst. Mag.*, vol. 17, no. 3, pp. 69–79, 1997.
[67] B. D. Coleman and M. L. Hodgdon, "A constitutive relation for rate-independent hysteresis in ferromagnetically soft materials," *Int. J. Eng. Sci.*, vol. 24, no. 6, pp. 897–919, 1986.
[68] P. Ge and M. Jouaneh, "Modeling hysteresis in piezoceramic actuators," *Precis. Eng.*, vol. 17, no. 3, pp. 211–221, 1995.
[69] I. D. Mayergoyz, *Mathematical Models of Hysteresis.* New York: Springer-Verlag, 1991.
[70] M. Brokate and J. Sprekels, *Hysteresis and Phase Transitions*. New York: Springer-Verlag, 1996.
[71] K. Kuhnen, "Modeling, identification and compensation of complex hysteretic nonlinearities: A modified Prandtl-Ishlinskii approach," *Eur. J. Control*, vol. 9, no. 4, pp. 407–418, 2003.
[72] T. Omata, S. Hara, and M. Nakano, "Nonlinear repetitive control with application to trajectory control of manipulators," *J. Robot. Syst.*, vol. 4, no. 5, pp. 631–652, 1987.
[73] H. Hikita, M. Yamashita, and Y. Kubota, "Repetitive control for a class of nonlinear systems," *JSME Int. J.*, vol. 36, no. 4, pp. 430–434, 1993.
[74] J. Ghosh and B. Paden, "Nonlinear repetitive control," *IEEE Trans. Autom. Control*, vol. 45, no. 5, pp. 949–953, 2000.
[75] X. Li, T. W. S. Chow, and J. K. L. Ho, "Quasi-sliding mode based repetitive control for nonlinear continuous-time systems with rejection of periodic disturbances," *Automatica*, vol. 45, no. 1, pp. 103–108, 2009.
[76] Y. Shan and K. K. Leang, "Accounting for hysteresis in repetitive control design: Nanopositioning example," *Automatica*, vol. 48, no. 8, pp. 1751–1758, 2012.
[77] R. D. Piner, J. Zhu, F. Xu, S. Hong, and C. A. Mirkin, "Dip-pen nanolithography," *Science*, vol. 283, no. 5402, pp. 661–663, Jan. 1999.
[78] R. Wiesendanger, *Scanning Probe Microscopy and Spectroscopy.* Cambridge, U.K.: Cambridge Univ. Press, 1994.
[79] Y. Li and Q. Xu, "A novel design and analysis of a 2-DOF compliant parallel micromanipulator for nanomanipulation," *IEEE Trans. Autom. Sci. Eng.*, vol. 3, no. 3, pp. 248–254, 2006.
[80] Y. Li and Q. Xu, "Design and analysis of a totally decoupled flexure-based XY parallel micromanipulator," *IEEE Trans. Robot.*, vol. 25, no. 3, pp. 645–657, 2009.
[81] L. M. Picco, L. Bozec, A. Ulcinas, D. J. Engledew, M. Antognozzi, M. A. Horton, and M. J. Miles, "Breaking the speed limit with atomic force microscopy," *Nanotechnology*, vol. 18, no. 4, article 044030, 2007.
[82] D. C. Jiles and D. L. Atherton, "Theory of ferromagnetic hysteresis," *J. Magn. Magn. Mater.*, vol. 61, nos. 1–2, pp. 48–60, 1986.
[83] H. J. M. T. A. Adriaens, W. L. de Koning, and R. Banning, "Modeling piezoelectric actuators," *IEEE/ASME Trans. Mechatron.*, vol. 5, no. 4, pp. 331–341, 2000.
[84] A. J. Fleming and S. O. R. Moheimani, "A grounded-load charge amplifier for reducing hysteresis in piezoelectric tube scanners," *Rev. Sci. Instrum.*, vol. 76, no. 7, article 073707, 2005.
[85] S. M. Hues, C. F. Draper, K. P. Lee, and R. J. Colton, "Effect of PZT and PMN actuator hysteresis and creep on nanoindentation measurements using force microscopy," *Rev. Sci. Instrum.*, vol. 65, no. 5, pp. 1561–1565, 1994.
[86] K. R. Koops, P. M. L. O. Scholte, and W. L. de Koning, "Observation of zero creep in piezoelectric actuators," *Appl. Phys. A*, vol. 68, no. 6, pp. 691–697, 1999.
[87] H. Jung and D.-G. Gweon, "Creep characteristics of piezoelectric actuators," *Rev. Sci. Instrum.*, vol. 71, no. 4, pp. 1896–1900, 2000.
[88] W. D. Callister, *Materials Science and Engineering: An Introduction*. New York: Wiley, 1994.
[89] G. Schitter, P. Menold, H. F. Knapp, F. Allgöwer, and A. Stemmer, "High performance feedback for fast scanning atomic force microscopes," *Rev. Sci. Instrum.*, vol. 72, no. 8, pp. 3320–3327, 2001.
[90] G. Schitter and A. Stemmer, "Fast closed loop control of piezoelectric transducers," *J. Vac. Sci. Technol. B*, vol. 20, no. 1, pp. 350–352, 2002.
[91] H. Janocha and K. Kuhnen, "Real-time compensation of hysteresis and creep in piezoelectric actuators," *Sens. Actuators A*, vol. 79, no. 2, pp. 83–89, 2000.
[92] H. Jung, J. Y. Shim, and D.-G. Gweon, "New open-loop actuating method of piezoelectric actuators for removing hysteresis and creep," *Rev. Sci. Instrum.*, vol. 71, no. 9, pp. 3436–3440, 2000.
[93] P. Krejci and K. Kuhnen, "Inverse control of systems with hysteresis and creep," *Proc. Inst Elec Eng. Control Theory Appl.*, vol. 148, no. 3, pp. 185–192, 2001.
[94] O. M. E. Rifai and K. Youcef-Toumi, "Creep in piezoelectric scanners of atomic force microscopes," in *Proc. American Control Conf.*, Anchorage, AK, May 8–10, 2002, pp. 3777–3782.
[95] A. E. Holman, P. M. L. O. Scholte, W. C. Heerens, and F. Tuinstra, "Analysis of piezo actuators in translation construction," *Rev. Sci. Instrum.*, vol. 66, no. 5, pp. 3208–3215, 1995.
[96] D. Croft and S. Devasia, "Vibration compensation for high speed scanning tunneling microscopy," *Rev. Sci. Instrum.*, vol. 70, no. 12, pp. 4600–4605, 1999.
[97] T. Sulchek, R. Hsieh, J. D. Adams, S. C. Minne, and C. F. Quate, "High-speed atomic force microscopy in liquid," *Rev. Sci. Instrum.*, vol. 71, no. 5, pp. 2097–2099, 2000.
[98] K. K. Leang and A. J. Fleming, "High-speed serial-kinematic AFM scanner: Design and drive considerations," in *Proc. American Control Conf.*, Seattle, WA, pp. 3188–3193, June 11–15, 2008.
[99] M. Tomizuka, T. C. Tsao, and K. K. Chew, "Discrete time domain analysis and synthesis of repetitive controllers," in *Proc. American Control Conf.*, Atlanta, GA, June 15–17, 1988, pp. 860–866.
[100] H. L. Broberg and R. G. Molyet, "Reduction of repetitive errors in tracking of periodic signals: Theory and application of repetitive control," in *Proc. 1st IEEE Conf. Control Applications*, Dayton, OH, Sept. 13–16, 1992 vol. 2, pp. 1116–1121.
[101] M. A. Janaideh, C.-Y. Su, and S. Rakheja, "Development of the rate-dependent Prandtl-Ishlinskii model for smart actuators," *Smart Mater. Struct.*, vol. 17, no. 3, article 035026, 2008.